ISSN 1063-7796, Physics of Particles and Nuclei, 2020, Vol. 51, No. 2, pp. 141–171. © Pleiades Publishing, Ltd., 2020.

To the memory of Milan Vymazal

Verification of z-Scaling in $p + p$, $\bar{p} + p$ and Au + Au Collisions at RHIC, Tevatron and LHC

M. V. Tokarev[a, c, *], I. Zborovský[b, **], A. O. Kechechyan[a, *], and T. G. Dedovich[a, c]**

[a] *Joint Institute for Nuclear Research, Dubna, 141980 Russia*

[b] *Nuclear Physics Institute, the Czech Academy of Science, Řež, 25068 Czech Republic*

[c] *Dubna State University, Dubna, 141980 Russia*

**e-mail: tokarev@jinr.ru*

***e-mail: zborovsky@ujf.cas.cz*

****e-mail: kechechyan@jinr.ru*

Received August 15, 2019; revised September 19, 2019; accepted September 19, 2019

Abstract—Experimental data on transverse momentum spectra of charged hadrons, strange particles, top quark and jets produced in $p + p$ and $\bar{p} + p$ collisions obtained at RHIC, Tevatron, and LHC are analyzed in the framework of z-scaling approach. The concept of the z-scaling based on fundamental principles of self-similarity, locality, and fractality of hadron interactions is verified over a wide range of collision energy and transverse momentum for different particle species. General properties of the data z-presentation are reviewed. A microscopic scenario of constituent interactions developed within the z-scaling scheme is used to study the dependence of momentum fractions and recoil mass on the collision energy, transverse momentum and mass of produced inclusive particle, and to estimate the constituent energy loss. Results of analysis in the framework of z-scaling of the negative particle spectra in Au + Au collisions obtained by the STAR Collaboration in the first phase of the Beam Energy Scan program at RHIC are presented. New indication on self-similarity of fractal structure of nuclei and fragmentation processes is found.

Keywords: high energy, proton, nuclei, jets, top quarks, strange particles, scaling

DOI: 10.1134/S1063779620020045

1. INTRODUCTION

Search for fundamental symmetries is main goal of all sciences and physics, in particular. Fundamental symmetry principles dictate the basic laws of physics, control the structure of matter, and define the fundamental forces in Nature [1]. Among them are principles of relativity (special, general, scale), gauge invariance, locality, self-similarity, spontaneous symmetry breaking and others.

The symmetries govern interactions of particles characterized with the properties such as mass, spin, charge and flavor. The interactions are studied in processes with leptons, hadrons and nuclei. The goal is to understand a complete picture of particle structure and their production mechanisms in terms of elementary constituent degrees of freedom. Flavor is one of the mysterious characteristics of hadrons. Six flavors of quarks (up, down, strange, charm, beauty and top) lead to a wide variety of mesons and baryons. Many experimental data allow both the study of properties of the particles and also their application as special probes to investigate collective phenomena in nuclear matter.

Different types of probes (high-p_T hadrons, direct photons, jets, leptons, strange and heavy flavor particles) play an important role to determine features of the produced matter and provide information about its transition into the observed particles. The hadron production with high transverse momenta is of a special interest. It has relevance to the particle substructure and constituent interactions at small scales and thus to discrete symmetries (C,P,T) of space-time and origin of their violation. While hard processes with high transverse momenta are used for testing the perturbative Quantum Chromodynamics (QCD), the multiple production of soft particles is suitable for verification of non-perturbative QCD and investigation of the phase transitions in non-Abelian theories. In the framework of QCD, the non-linear Yang–Mills equations taking into account gauge invariance and Lorentz covariance regulate dynamics of the constituent interactions both at hard and soft regimes. The quark-gluon system produced in these interactions undergoes a phase transition to the colorless hadrons. A detailed understanding of the hadronization is still an open problem and its description relies mostly on phenomenology.

It is well known that all physical systems should reveal discontinuity in some characteristics describing their behavior nearby a phase boundary or a critical point. Therefore the concepts of "scaling" and "universality" have been developed and widely used to explain the critical phenomena [2–5]. Scaling implies that systems near critical points exhibit self-similarity and are invariant with respect to scale transformations. The universality of their behavior lies in the fact that vastly different systems behave in a similar way near respective critical point which is usually described by a power dependence. The critical exponents in the power laws are determined by the interaction symmetry and space dimension only. The notions of scaling and universality have also been applied for particle production far from the boundary of a phase transition or a critical point. In high energy collisions, the scaling regularities were subject of intense investigations [6–23]. Such regularities reflect usually some symmetry principles. Their violation can give experimental indications on new physics phenomena and additional insight into theory.

One of the fundamental principles governing hadron interactions at high energies is the self-similarity principle. Its relation to the scale relativity and fractal properties of the quantum space-time are discussed in [24–26]. The scaling behavior related to the ideas of self-similarity of hadron interactions at a constituent level is manifested by the z-scaling [27–31]. The scaling was used for analysis of inclusive spectra obtained at the accelerators U70, S$\bar{\text{p}}$pS, SPS, ISR, Tevatron, and RHIC [32–47].

The transverse momentum spectra reveal striking similarity over a wide range of energies when expressed by the variable z. The scaling is treated as a manifestation of the self-similarity of the structure of the colliding objects (hadrons or nuclei), the interaction mechanism of their constituents, and the process of fragmentation into real hadrons. Universality of the z-scaling is given by its flavour independence. It means that spectra of particles with different flavour content can be described by the same function $\psi(z)$ with values of z and ψ rescaled by a multiplicative factor α_F. The factor was found to be constant over a wide kinematic range. The z-scaling was confirmed in the region which is far from boundary of a phase transition or the region where a critical point can be located. We consider that the approach can be a suitable tool to search for a phase transition or critical point in hadron and nuclear matter at energies where the Beam Energy Scan (BES) program is being currently performed at RHIC [48–50].

2. z-SCALING: GENERAL APPROACH

In this paper we follow the z-scaling version presented in [27]. Let us briefly remind the basic ideas of this concept. At high energies, the collision of two hadrons or nuclei is considered as an ensemble of individual interactions of their constituents. The constituents are formed from partons in the parton model or consist of quarks and gluons in the QCD theory. Structures of the colliding objects are characterized by parameters δ_1 and δ_2. The interacting constituents carry the fractions x_1 and x_2 of the momenta P_1 and P_2 of the colliding hadrons (or nuclei), respectively. The inclusive particle carries the momentum fraction y_a of the scattered constituent with fragmentation characterized by a parameter ϵ_a. A fragmentation of the recoil constituent is described by ϵ_b and the momentum fraction y_b. Multiple interactions are considered to be similar. This property represents self-similarity of the hadron interactions at the constituent level.

The constituent picture of hadron interactions at high energies provides the basis for analyzing inclusive spectra of particles produced in proton and nuclei collisions in the framework of z-scaling approach. The self-similar properties of the interactions are manifested by the observation that invariant differential cross sections of particles of different types can be described in terms of a scaling function $\psi(z)$ and the scaling variable z over a wide kinematic range.

2.1. A Microscopic Scenario of Hadron Production

According to ideas of unified description of inclusive cross sections at high energies [12], the gross features of momentum distributions of an inclusive particle h produced in the collisions

$$A_1 + A_2 \to h + X \tag{1}$$

of the extended objects like hadrons or nuclei with the atomic numbers A_1 and A_2 can be expressed in terms of the kinematic characteristics of a corresponding constituent sub-process. We consider the sub-process to be a binary collision of the constituents with masses (x_1M_1) and (x_2M_2) which results in the scattered and recoil objects in the final state with masses (m_a/y_a) and $(x_1M_1 + x_2M_2 + m_b/y_b)$, respectively. The constituents of the incoming hadrons (or nuclei) with masses M_1, M_2 and momenta P_1, P_2 carry their fractions x_1, x_2. The produced secondary objects transform into real particles after the constituent collisions. The registered particle with mass m_a and the 4-momentum p carries the fraction y_a of the 4-momentum of the scattered constituent. Its hadron counterpart with mass m_b, moving in the opposite direction, carries the y_b fraction of the produced recoil. The momentum conservation law in the constituent sub-process is connected with the recoil mass $M_X = x_1M_1 + x_2M_2 + m_b/y_b$ as follows

$$(x_1P_1 + x_2P_2 - p/y_a)^2 = M_X^2. \tag{2}$$

The associate production of the particle with the mass m_b ensures conservation of the additive quantum numbers (the electric charge, baryon number, strangeness, charm, beauty). Equation (2) is an expression of the locality of the hadron interaction at a constituent level. It poses a constraint on the momentum fractions x_1, x_2, y_a, and y_b which determine the constituent sub-process.

Structure of the colliding objects and fragmentation of the systems moving in the scattered and recoil directions is characterized by the structural parameters δ_1, δ_2, and ϵ_a, ϵ_b, respectively. We connect the parameters with the corresponding momentum fractions by the function

$$\Omega = (1 - x_1)^{\delta_1}(1 - x_2)^{\delta_2}(1 - y_a)^{\epsilon_a}(1 - y_b)^{\epsilon_b}. \quad (3)$$

Physical meaning of Ω is given by its proportionality to relative number of all such constituent configurations in the reaction (1) which contain the configuration defined by the fractions x_1, x_2, y_a, and y_b. The function Ω plays the role of a relative volume which occupy these configurations in space of the momentum fractions. The structural parameters δ_1, δ_2, ϵ_a, and ε_b are interpreted as fractal dimensions in the respective parts of the considered space of momentum fractions. The fractal structure of the colliding hadrons (nuclei) is characterized by δ_1 and δ_2. The fractal nature of the fragmentation processes in final state is described by ϵ_a and ϵ_b.

The value of $\Omega^{-1}(x_1, x_2, y_a, y_b)$ describes a resolution at which the sub-process defined by x_1, x_2, y_a, and y_b can be singled out of the inclusive reaction. For given values of δ_1, δ_2, ϵ_a, and ε_b, the momentum fractions x_1, x_2, y_a, and y_b are determined in a way to maximize the function $\Omega(x_1, x_2, y_a, y_b)$, simultaneously fulfilling condition (2). The requirement of the minimal resolution Ω^{-1} singles out the corresponding underlying interaction of constituents which satisfies the condition (2). The maximal value of Ω is used in the definition (4) of the scaling variable z.

The parameters ϵ_a and ϵ_b enable to take effectively into account also prompt resonances out of which the inclusive particle of a given type may be created. At fixed masses m_a and m_b, larger values of ϵ_a and ϵ_b correspond to smaller y_a and y_b, which in turn give larger ratios m_a/y_a and m_b/y_b. In our phenomenological approach this means that production of the inclusive particle with mass m_a and its counterpart with mass m_b can be a result of fragmentation from larger masses which mimic in a sense processes with prompt resonances.

2.2. Self-Similarity Variable z and Scaling Function $\psi(z)$

The self-similarity of hadron interactions reflects a property that hadron constituents and their interactions are similar. The self-similarity variable z is defined as follows

$$z = z_0\Omega^{-1}. \quad (4)$$

Here

$$z_0 = \frac{\sqrt{s_\perp}}{(dN_{\rm ch}/d\eta|_0)^c m_N}, \quad (5)$$

and Ω is maximal value of (3) with the condition (2). The variable z_0 is proportional to the transverse kinetic energy $\sqrt{s_\perp}$ of the constituent sub-process consumed on the production of the inclusive particle (m_a) and its counterpart (m_b). The quantity $dN_{\rm ch}/d\eta|_0$ is the corresponding multiplicity density of charged particles produced in the central region of the reaction (1) at pseudo-rapidity $\eta = 0$. The value of $dN_{\rm ch}/d\eta|_0$ is raised to the power of c in (5). The multiplicity density in the central interaction region is related to a state of the produced medium. The parameter c characterizes properties of this medium [27]. It is determined from multiplicity dependence of inclusive spectra [45]. The arbitrary mass constant m_N is fixed at the value of nucleon mass. The variable z is a function of the momentum fractions (x_1, x_2, y_a, y_b), multiplicity density, and depends on the parameters $\delta_1, \delta_2, \epsilon_a, \epsilon_b$, and c.

The scaling function $\psi(z)$ is expressed in terms of the experimentally measured inclusive invariant cross section $Ed^3\sigma/dp^3$, the multiplicity density $dN/d\eta$ and the total inelastic cross section $\sigma_{\rm in}$ as follows [31]

$$\psi(z) = \frac{\pi}{(dN/d\eta)\sigma_{\rm inel}} J^{-1} E\frac{d^3\sigma}{dp^3}, \quad (6)$$

where J is the Jacobian for the transformation from $\{p_T^2, y\}$ to $\{z, \eta\}$. The Jacobian depends on kinematic variables characterizing the inclusive process (1). The multiplicity density $dN/d\eta$ in the expression (6) concerns particular hadrons species. It depends on the center-of-mass energy, on various multiplicity selection criteria and also on the production angles at which the inclusive spectra were measured. The function $\psi(z)$ is normalized to unity,

$$\int_0^\infty \psi(z)dz = 1. \quad (7)$$

The relation allows us to interpret $\psi(z)$ as a probability density to produce an inclusive particle with the corresponding value of the self-similar variable z.

Flavor independence of the z-presentation of inclusive spectra means that the shape of the scaling function $\psi(z)$ is the same for hadrons with different flavor content over a wide range of the variable z [28]. The scale transformation

$$z \to \alpha_F z, \quad \psi \to \alpha_F^{-1}\psi \tag{8}$$

is used for comparison of the shapes of the scaling function for different hadron species. The scale parameter α_F is a constant independent of kinematic variables. Its values depend on type of the produced particles. The transformation does not change the shape of $\psi(z)$. It preserves the normalization condition (7) and does not destroy the energy, angular, and multiplicity independence of the z-presentation of particle spectra.

3. z-SCALING IN $p + p$ COLLISIONS

Particle production in $p + p$ collisions is interesting both for itself and for comparison with $p + A$ and $A + A$ collisions. In the first case the constituent interactions are not influenced by the nuclear medium and features of hadron substructure, interaction and fragmentation manifest themselves more clear. In the second case the nuclear medium can essentially modify the elementary sub-processes and signatures of phase transitions are expected to occur.

Here we remind main features of the z-scaling in $p + p$ interactions. For the unpolarized proton-proton collisions we have $\delta_1 = \delta_2 \equiv \delta$. We assume that objects produced in constituent sub-processes in the scattered and recoil directions have equal fragmentation properties which can be described by the same parameter $\epsilon_a = \epsilon_b \equiv \epsilon$. For identified particles, the fragmentation dimension depends on type of the inclusive particle, $\epsilon = \epsilon_F$, which we denote by the subscript F. The scaling of inclusive hadrons was established [27, 28, 47] from analyses of data measured at FNAL, CERN, and BNL energies for constant values of δ and ϵ_F. The experimental data cover a wide range of the collision energy and transverse momentum of produced particles.

3.1. h^- Hadrons

Figure 1a shows the energy independence of the scaling function $\psi(z)$ for h^- hadron production in $p + p$ collisions over a wide range of collision energy $\sqrt{s}$ = 11.5, 19.4, 27.4, 38.8, 62, 63, and 200 GeV in the transverse momentum interval p_T = 0.2–13 GeV/c at $\theta_{cms} \simeq 90°$ [51–57]. The function $\psi(z)$ changes by more than twelve orders of magnitudes.

The energy independence of the scaling function gives strong constraints on the values of the parameters c, δ and ϵ. The z-scaling is consistent with the constant values of the parameters $c = 0.25$, $\delta = 0.5$, and $\epsilon = 0.2$ for $\sqrt{s} \geq 19$ GeV. At the energy $\sqrt{s} = 11.5$ GeV, the scaling regularity indicates a decrease of δ and ϵ. The diminishing of the fractal dimensions is naturally expected due to a smearing of the fractal character of hadron interactions at low energies. As seen from Fig. 1a, the behavior of $\psi(z)$ can be described by a power law, $\psi(z) \sim z^{-\beta}$, in the asymptotic high-z (high-p_T) region. A characteristic saturation of the scaling function is observed at low z (low p_T). The results are in agreement with similar observations for identified particles presented in [27, 28, 47].

Figure 1b demonstrates the dependence of the momentum fraction x_1 on the transverse momentum p_T of negative hadrons produced in $p + p$ collisions at $\sqrt{s}$ = 11.5–200 GeV and $\theta_{cms} \simeq 90°$. The values of $x_1 (\simeq x_2)$ characterize energy of the constituent sub-process which underlies production of the inclusive particle. The momentum fraction x_1 demonstrates monotonic growth with p_T. It decreases with the increasing collision energy $\sqrt{s}$. For a given transverse momentum (e.g. p_T = 4 GeV/c), the largest fraction ($x_1 \simeq 0.8$) corresponds to the lowest energy $\sqrt{s}$ = 11.5 GeV. The kinematic limit of the reaction is reached at $x_1 = 1$.

Figure 1c shows the dependence of the fraction y_a on the transverse momentum p_T of the produced particle. The relative energy loss of the scattered constituent with energy E_q is given by the relation $\Delta E_q / E_q = (1 - y_a)$. As seen from Fig. 1c, all points demonstrate non-linear monotonic growth of y_a with p_T. This means that the relative energy dissipation associated with a high-p_T particle is smaller than for the inclusive particle with lower transverse momentum. For a given p_T, the energy loss is larger at higher energy because the corresponding fraction y_a decreases with $\sqrt{s}$. For the collision energy $\sqrt{s}$ = 200 GeV, the energy loss is estimated to be about 65 and 40% at p_T = 4 and 13 GeV/c, respectively. At p_T = 4 GeV/c, the energy loss falls to around 5% at $\sqrt{s}$ = 11.5 GeV.

The recoil object in the corresponding sub-process moves in the away side direction of the inclusive particle. The object is characterized by the recoil mass M_X. Figure 1d shows the dependence of M_X on the transverse momentum p_T of negative hadrons produced in $p + p$ collisions in the same range of collision energy. The single points demonstrate a growth at low p_T followed by a successive flattening. The values of M_X reveal characteristic increase with $\sqrt{s}$. The recoil mass is about 6–7 GeV at the energy $\sqrt{s}$ = 200 GeV and momentum p_T = 13 GeV/c. At $\sqrt{s}$ = 11.5 GeV, the recoil mass is about $M_X \simeq 2.1$ GeV/c^2 for the highest measured p_T = 4 GeV/c.

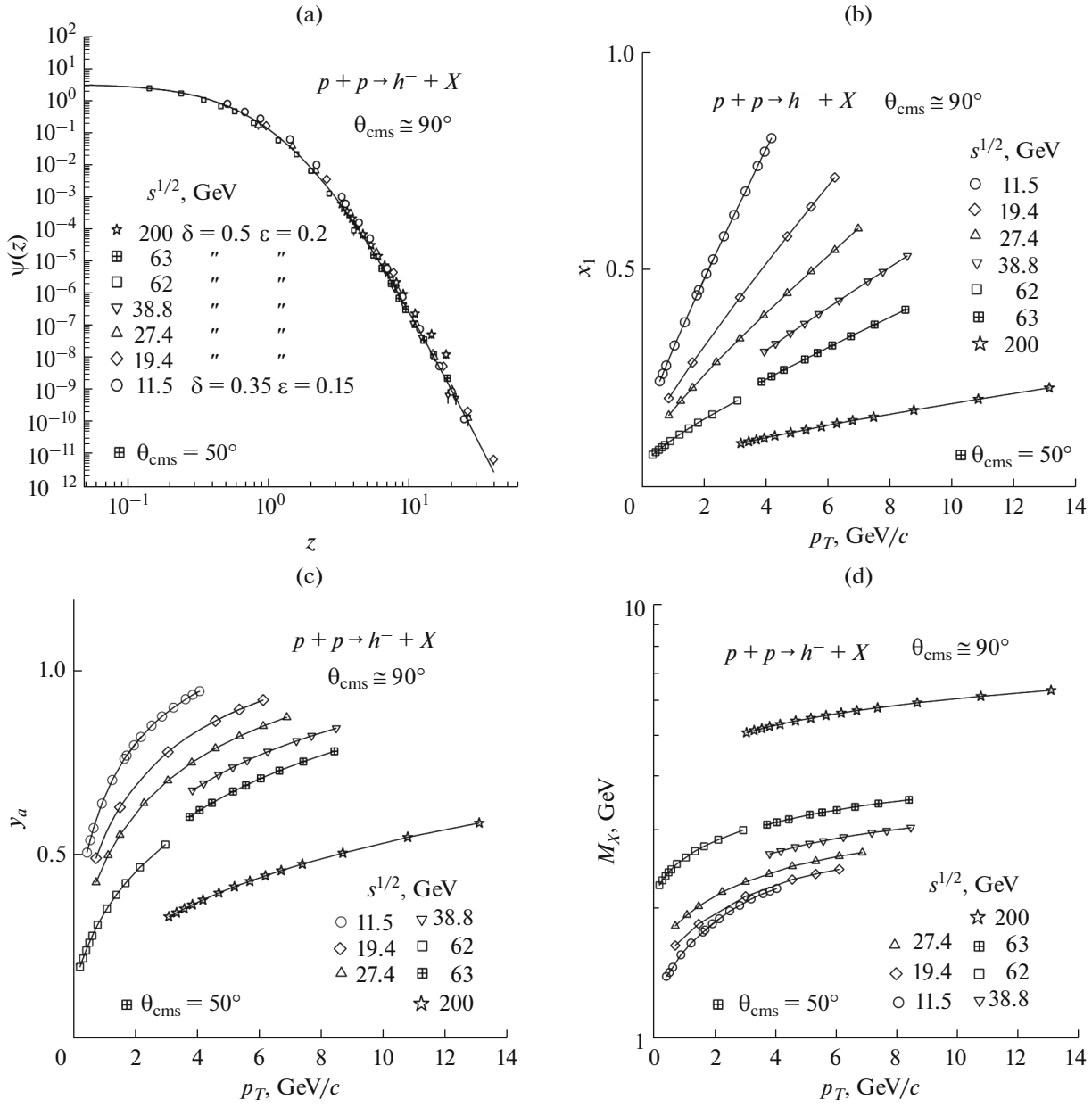

Fig. 1. Scaling function $\psi(z)$ (a), momentum fractions x_1 (b), y_a (c), and recoil mass M_X (d) for negative hadrons produced in $p + p$ collisions at $\sqrt{s} = 11.5$–200 GeV and $\theta_{cms} \simeq 90°$. The symbols correspond to the experimental data [51–57] measured at the CERN, FNAL, and BNL. The solid line shown in (a) is a reference curve.

3.2. Identified $\pi, K, \bar{p}$ Particles

Figure 2a shows the z-presentation of the spectra of negative pions, kaons, antiprotons, and Λ's produced in $p + p$ collisions over the range $\sqrt{s} = 19$–200 GeV and $\theta_{cms} = 3°$–$90°$. The symbols represent data on differential cross sections measured in the central and fragmentation regions [51–57]. The analysis comprises the inclusive spectra of particles measured up to very small transverse momenta ($p_T \simeq 45$ MeV/c for pions and $p_T \simeq 120$ MeV/c for kaons or antiprotons). One can see that the distributions of different hadrons are sufficiently well described by a single curve over a wide z-range (0.01–30). The function $\psi(z)$ changes more than twelve orders of magnitude. The solid lines represent the same curve shifted by multiplicative factors for reasons of clarity. The same holds for the corresponding data shown with the different symbols. The indicated values of the parameter ϵ_F ($\varepsilon_\pi = 0.2$, $\epsilon_K \simeq 0.3$, $\epsilon_{\bar{p}} \simeq 0.35$, $\epsilon_\Lambda \simeq 0.4$) are consistent with the

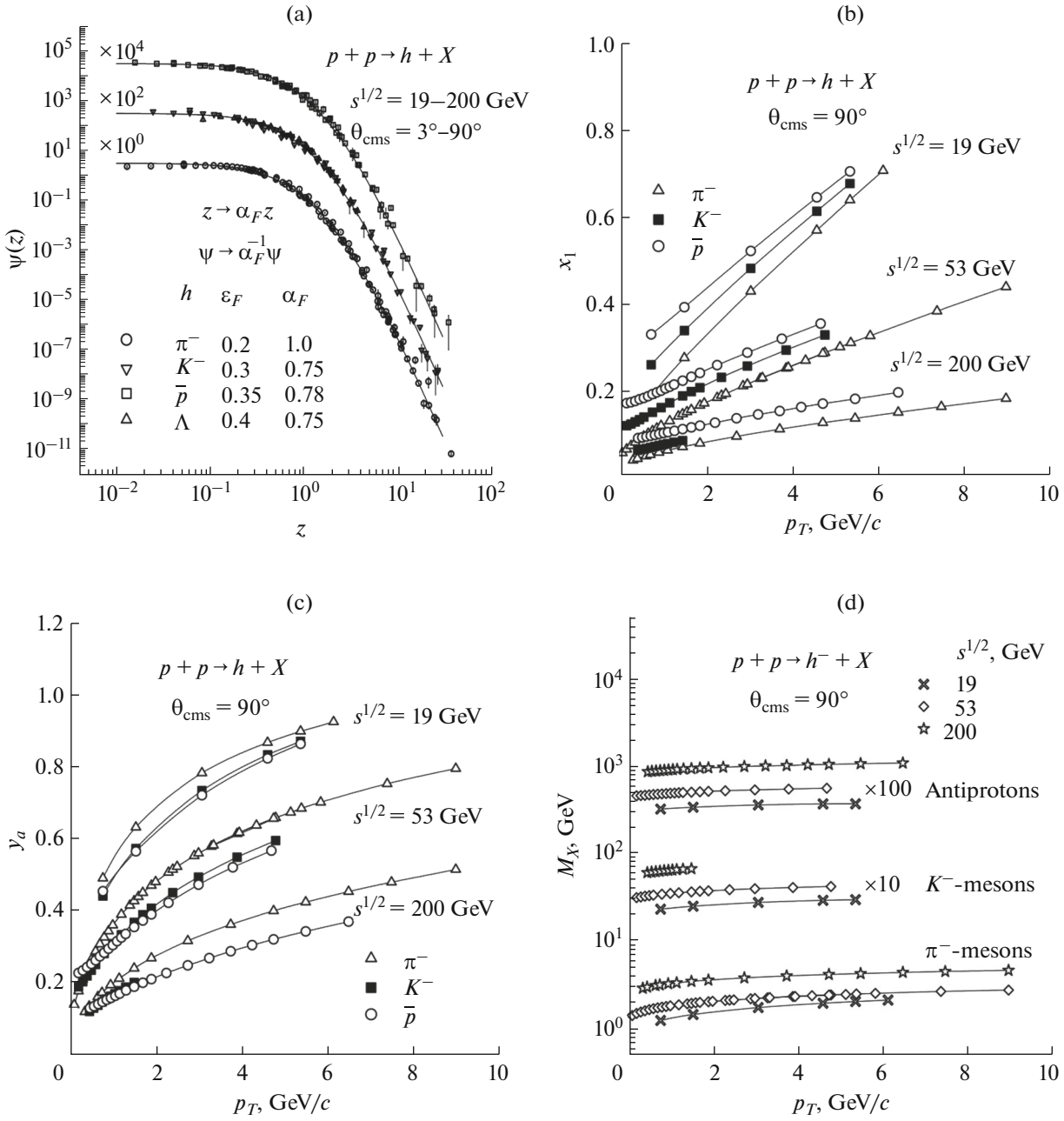

Fig. 2. Scaling function $\psi(z)$ (a) for $\pi^-, K^-, \bar{p}$, and Λ hadrons produced in $p + p$ collisions at $\sqrt{s} = 11.5$–200 GeV and $\theta_{cms} \simeq 90°$ (a). The dependence of the fractions x_1 (b), y_a (c), and recoil mass M_X (d) on the transverse momentum p_T for π^-, K^-, and $\bar{p}$ produced in the $p + p$ collisions at $\sqrt{s} = 19, 53$, and 200 GeV. The symbols correspond to the experimental data [51–57] measured at the CERN, FNAL, and BNL. The solid line shown in (a) is a reference curve.

energy, angular, and multiplicity independence of the z-presentation of spectra for different hadrons. The parameters were found to be independent of kinematical variables ($\sqrt{s}$, p_T, and θ_{cms}). The scale factors α_F are constants which allow us to describe the z-presentation for different hadron species by a single curve. The estimated errors of α_F are at the level of 20%.

Figure 2b shows the dependence of the fraction x_1 on the transverse momentum p_T of the negative pions, kaons, and antiprotons produced in $p + p$ collisions at $\sqrt{s} = 19, 53, 200$ GeV and $\theta_{cms} = 90°$. The fractions x_1 and x_2 are equal each other in that case. They increase nearly linearly with the transverse momentum p_T. For fixed p_T, the fraction x_1 decreases as the collision

energy $\sqrt{s}$ increases. The x_1 is larger for the production of heavy particles as compared with light ones. The kinematical limit of the reaction (1) corresponds to $x_1 = x_2 = 1$ at any collision energy and for any type of the inclusive particle. This can be seen in Fig. 2 for $\sqrt{s} = 19$ GeV where the fraction x_1 approximates unity at $p_T \simeq 9$ GeV/c for all three particles.

The dependence of the momentum fractions y_a and y_b on the kinematical variables $(p_T, \theta_{\text{cms}}, \sqrt{s})$ describes features of the fragmentation process. The fraction y_a characterizes dissipation of the energy and momentum of the object produced by the underlying constituent interaction into the near side of the inclusive particle. This effectively includes energy losses of the scattered secondary partons moving in the direction of the registered particle as well as feed down processes from prompt resonances out of which the inclusive particle may be created. The fraction y_b governs the recoil mass in the constituent sub-process. Its value characterizes the dissipation of the energy and momentum in the away side direction of the inclusive particle.

Figure 2c shows the dependence of y_a on the transverse momentum p_T for the negative pions, kaons, and antiprotons produced in $p + p$ collisions at the energy $\sqrt{s}$ = 19, 53, 200 GeV and $\theta_{\text{cms}} = 90°$. All curves demonstrate a non-linear monotonic growth with p_T. It means that the energy dissipation associated with the production of a high-p_T particle is smaller than for the inclusive processes with lower transverse momenta. This feature is similar for all inclusive reactions at all energies. The decrease of the fractions y_a with the increasing collision energy is another property of the considered mechanism. It corresponds to more energy dissipation at higher energies. This can be due to the larger energy losses and/or due to the heavy prompt resonances. The third characteristic is a slight decrease of y_a with the mass of the inclusive particle. It implies more energy dissipation for creation of heavier hadrons as compared with hadrons with smaller masses. The asymptotic value of $y_a = 1$ is reached at the kinematical limit for all particle species.

The dependence of the momentum fraction y_b on p_T reflects kinematic properties of the recoil system. The values of y_b are larger for particles with higher masses. It was found that y_b is nearly independent of p_T in the studied region. It is smaller than y_a and decreases with the increasing collision energy $\sqrt{s}$. The small values of y_a mean that the momentum balance in the production of an inclusive particle from a subprocess is more likely compensated with many particles with smaller momenta than by a single particle with a higher momentum moving in the opposite direction.

Figure 2d shows the dependence of the recoil mass M_X on the transverse momenta of the negative pions, kaons, and antiprotons produced in $p + p$ collisions at the energy $\sqrt{s} = 19$, 53, and 200 GeV in the central rapidity region. For the sake of clarity, the values of M_X are presented on a log-scale with the multiplication factors 10 and 100 for K^- and $\bar{p}$, respectively. All curves demonstrate small growth at low p_T followed by a successive flattening. They reveal a characteristic increase with the collision energy and mass of the inclusive particle.

3.3. Strange Hadrons

The strange particles represent a special interest as they contain strange quarks which are the lightest quarks absent in the net amount in the initial state. At the same time, the strange quarks created in the constituent sub-processes are substantially heavier than the valence quarks in the colliding protons. The self-similarity of such interactions, expressed by the same form of the scaling function, results in different properties of the constituent collisions and fragmentation processes as compared to those which underlay the production of the non-strange particles. Therefore, the scaling behavior of $\psi(z)$ found in data analysis of inclusive reactions with strange particles could give more evidence in support of unique description of $p + p$ interactions at constituent level and can provide good grounds for study of peculiarities of the strangeness production in nuclear collisions. For investigation of fractal properties of the strange quarks, it is important to estimate the energy loss and also the scale at which the constituent sub-processes are singled out for a given inclusive reaction. These conditions are controlled by the dependence of the variable z on the multiplicity density, collision energy, transverse momentum and also on the angle at which the inclusive particle is detected.

Figure 3a shows z-presentation [47] of the transverse momentum spectra of strange mesons and baryons measured in $p + p$ collisions at $\sqrt{s} = 200$ GeV in the central rapidity region at RHIC. The symbols representing data on differential cross sections include baryons which consist of one, two and three strange valence quarks. The multiplicative factors $10^0, 10^{-1}$ and 10^{-2} are used to show the data z-presentation separately for mesons, single-strange $(\Lambda, \Lambda^*, \Sigma^*)$ and multi-strange (Ξ^-, Ω) baryons, respectively.

The open circles and diamonds correspond to the respective spectra of K^0_S and K^- mesons measured by the STAR Collaboration [57, 58]. The data on the neutral short-lived $K^{*0}(892)$ resonance obtained by the STAR [59] and PHENIX [60] Collaborations are

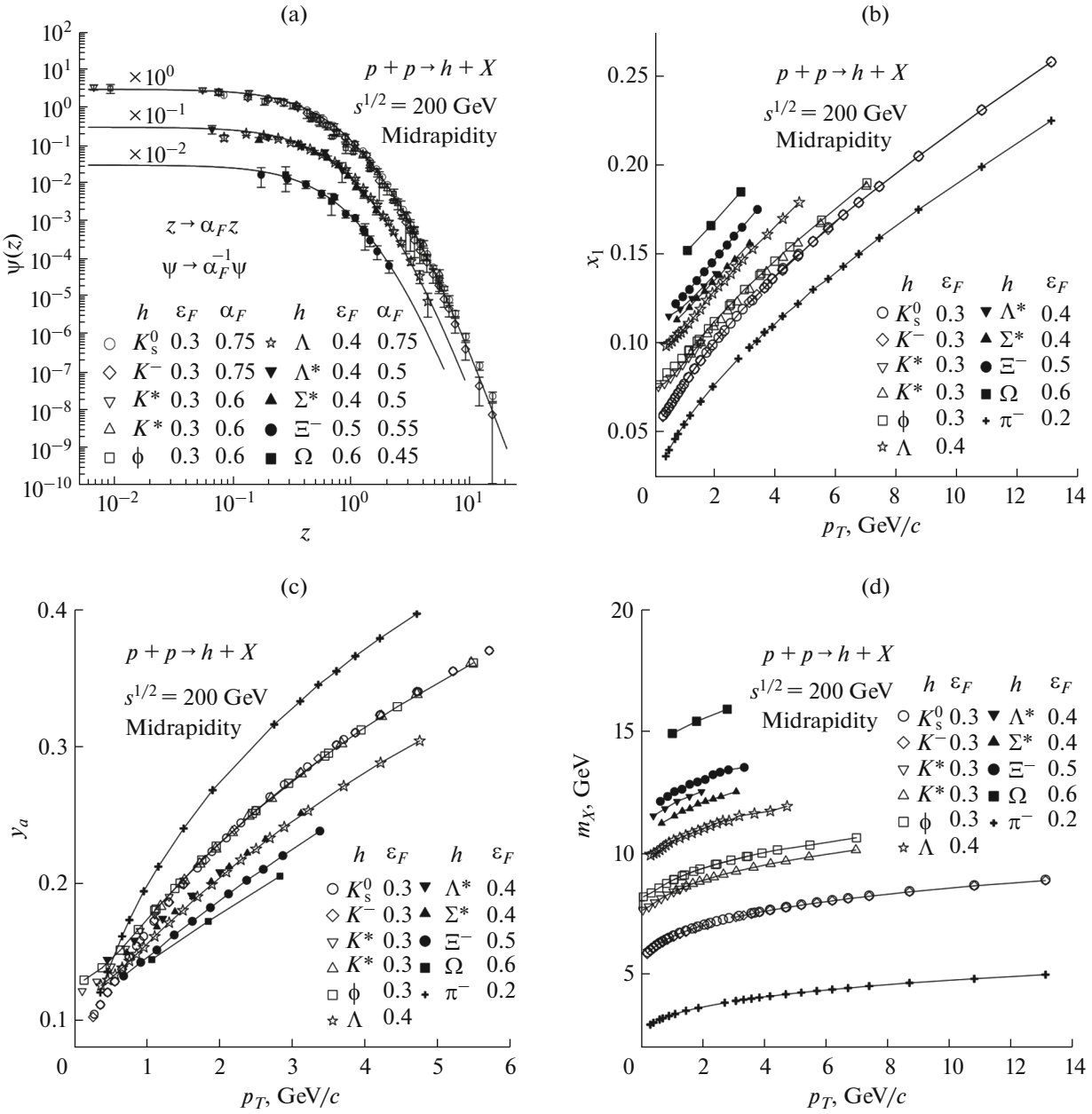

Fig. 3. Scaling function $\psi(z)$ (a), momentum fractions x_1 (b), y_a (c), and recoil mass M_X (d) for strange ($K^0_S, K^-, K^{*0}, \phi, \Lambda, \Lambda^*, \Sigma^*, \Xi^-, \Omega$) hadrons produced in $p + p$ collisions at $\sqrt{s} = 200$ GeV and $\theta_{\rm cms} \simeq 90°$ [47]. Experimental data are taken from [58–62]. The solid line in (a) is fit of $\psi(z)$ for π^- mesons [63]. The points in (b), (c), (d) are calculated for $\delta = 0.5$ and for the indicated values of ϵ_F.

depicted by the triangles down and triangles up, respectively. The open squares correspond to the PHENIX data on ϕ-meson production [61] detected in the K^+K^- and e^+e^- decay channels. The z-presentation of spectra of strange baryons shown in the figure is based on the data collected by the STAR Collaboration [58]. The distributions of Λ, Ξ^- and Ω baryons are depicted by stars, black circles and black squares, respectively. The spectra of strange baryon resonances $\Sigma^*(1385)$ (full triangles up) and $\Lambda^*(1520)$ (full triangles down) were taken from [62]. The solid line represents the scaling curve obtained from analysis of pion spectra [57, 63] in $p + p$ collisions ($\epsilon_\pi = 0.20 \pm 0.01$) over a wide range of kinematic variables [28]. The line is used as a reference ($\alpha_\pi = 1$) for comparison with other particles. The data on strange particle spectra [53, 54,

64–72] obtained by the BS, CCRS, CDHW, AFS, NA61/SHINE, NA49 and STAR Collaborations were also used in the analysis. The data points for different particles are shown for the values of the parameters α_F and ϵ_F indicated in Fig. 3a. They correspond to the scaling behavior of $\psi(z)$. Note that the spectra for Ξ^- and Ω baryons were measured at $\sqrt{s} = 200$ GeV only and in a limited p_T-region. Therefore, the data does not allow unique determination of ϵ_F and α_F. More measurements at different energies and in a wider p_T-range could contribute to unambiguous determination of the parameters.

We estimate the errors of ϵ_F and α_F for K^0_S, K^-, K^{*0}, ϕ, and Λ particles at the level 10%. The errors of the parameters for $\Lambda^*, \Sigma^*, \Xi^-$ hyperons are up to 20%, and for Ω are difficult to assess. They depend on the fitting z-range. A small number of data points for multi-strange baryons allow us to find the corresponding parameters in a narrow range of z only. As seen from Fig. 3a, the data points for $\Lambda^*, \Sigma^*, \Xi^-, \Omega$ hyperons are reasonably well described by the solid curve with the given values of ϵ_F and α_F. The curve is consistent with the energy, angular and multiplicity independence of the scaling function for different hadrons. One can see that the corresponding fragmentation dimension ϵ_F for strange mesons is larger than for pions, suggesting larger energy loss by production of mesons with strangeness content. The fragmentation dimension for strange baryons grows with the number of the strange valence quarks.

Figure 3b shows p_T-dependence of the momentum fraction x_1 for production of different strange hadrons and π^- mesons. For a given strangeness and p_T, x_1 increases with the mass of the strange hadron. Due to the larger energy loss and recoil mass by production of hadrons with strange quark content relative to π^- mesons, the values of x_1 are higher for strange hadrons as compared to those corresponding to pions.

The p_T-dependence of the momentum fraction y_a of strange hadrons and π^- mesons produced in $p + p$ collisions at $\sqrt{s} = 200$ GeV is shown in Fig. 3c. The fraction y_a increases with p_T for all particles. The relative energy loss $\Delta E_q / E_q = (1 - y_a)$ depends on value of the fragmentation dimension ϵ_F. As one can see, the energy loss decreases with increasing p_T for all particles. For a given $p_T > 1$ GeV/c, the energy loss is larger for strange baryons than for strange mesons. The growth indicates increasing tendency with larger number of strange valence quarks inside the strange baryon $(\Delta E/E)_\Omega > (\Delta E/E)_{\Xi^-} > (\Delta E/E)_\Lambda \simeq (\Delta E/E)_{\Lambda^*} \simeq (\Delta E/E)_{\Sigma^*}$.

The p_T-dependence of the recoil mass M_X for various strange hadrons is illustrated in Fig. 3d. The values of M_X reveal characteristic growth with transverse momentum for all particles. For a given p_T, the recoil mass M_X increases with meson masses $M_X(\phi) > M_X(K^{*0}) > M_X(K^0_S) \simeq M_X(K^-) > M_X(\pi^-)$. One can see the similar tendency for Ω, Ξ^- and Λ baryons as well.

3.4. Top Quark

The *top*-quark is the heaviest known elementary particle. It was discovered at the Tevatron $\bar{p} + p$ collider in 1995 by the CDF and DØ Collaborations [73, 74] at a mass of around 170 GeV. The first measurements of the differential cross section as a function of the transverse momentum of the *top*-quark were presented by the DØ Collaboration in [75]. It is expected that *top* physics is extremely important to search for new and study of known symmetries in high-p_T region. The first analysis of *top*-quark spectra [75] in the framework of the z-scaling approach was performed in [34]. Here we present results of analysis of spectra of *top*-quark production obtained at the LHC and compare it with data at lower energy from the Tevatron. The differential cross sections were measured in dependence on the *top*-quark transverse momentum p_T at mid-rapidity.

Figure 4 shows the z-presentation of the spectra of *top*-quark production obtained in $p + p$ collisions at the LHC energies $\sqrt{s} = 7$, 8 and 13 TeV in the central rapidity region. The data were obtained by the CMS [76–79] and ATLAS [80–83] Collaborations. The measurements of the inclusive production cross section were performed in the dilepton and jet channels. The data include measurements over a wide range of the transverse momentum $30 < p_T < 1000$ GeV. The scaling function $\psi(z)$ for the *top*-quark distributions was calculated according to (6). Data on π^--meson spectra shown by the solid line serves as a reference data. The values of the fractal dimension $\delta = 0.5$ and the parameter $c = 0.25$ are the same as used in our previous analyses [27, 28]. We have set $\epsilon_{top} = 0$ in the case of the *top*-quark, as no or negligible energy loss is assumed in the elementary $t\bar{t}$ production process. This choice corresponds to $y_a = y_b = 1$ in the whole p_T-range. The scale parameter α_F in the transformation (8) is found to be $\alpha_{top} \simeq 0.0045$. No additional parameters were used. The data [84] on the *top*-quark production in $\bar{p} + p$ collisions obtained by the DØ Collaboration at the Tevatron energy $\sqrt{s} = 1.96$ TeV are shown for comparison with the data measured at the LHC. The scaling function demonstrates energy independence over a wide range of the self-similarity

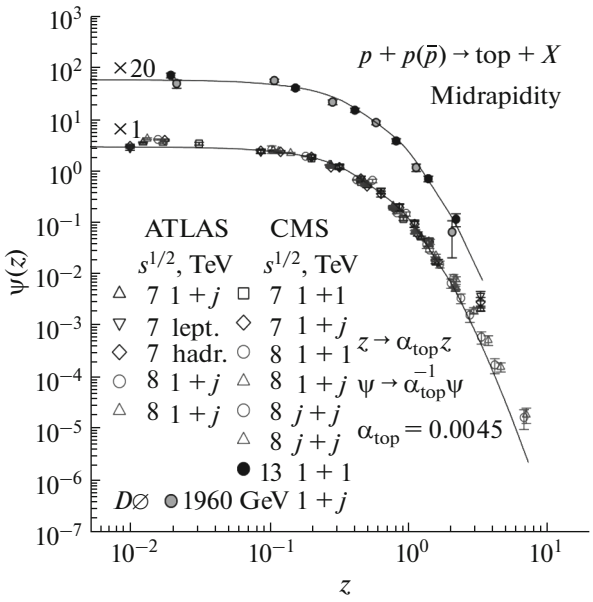

Fig. 4. The scaling function $\psi(z)$ of the *top*-quark production in $p + p$ and $p + \bar{p}$ collisions at the LHC energies $\sqrt{s} = 7, 8, 13$ TeV and at the Tevatron energy $\sqrt{s} = 1.96$ TeV. The symbols denote the experimental data obtained by the CMS [76–79], ATLAS [80–83] and DØ [84] Collaborations. The solid line is a reference curve corresponding to π^--meson production in $p + p$ collisions.

parameter $z = 0.01$–8. The function $\psi(z)$ changes more than five orders of magnitude in this region.

As seen from Fig. 4, the z-presentation of the *top*-quark transverse momentum distributions follows the shape of the z-scaling curve in $p + p$ ($\bar{p} + p$) collisions for other particles sufficiently well. Though the *top* spectrum is in the limited kinematic region, we would like to stress that it is compared with existing analyses of p_T-distributions of inclusive cross sections $Ed^3\sigma/dp^3$ for other hadrons which reveal strong dependence on the energy, angle, multiplicity, and type of the produced particles. Based on the above comparison we conclude that the new LHC and Tevatron data on inclusive spectra of the *top*-quark production support the flavor independence of the scaling function $\psi(z)$ over the interval of $z = 0.01$–8. This result gives us indication on self-similarity of *top*-quark production in $p + p$ and $\bar{p} + p$ interactions up to the *top*-quark transverse momentum $p_T < 1000$ GeV and for a wide range of the collision energies $\sqrt{s}$.

3.5. Jets

Jets are traditionally considered as a best probe of constituent interactions at high energies. They are of interest both for study of jet properties itself and in search for new particles identified by the jets. In hadron collisions, jet is a direct evidence of hard interaction of hadron constituents (quarks and gluons). The inclusive jet cross section measures the probability of observing a hadronic jet as a sign of a hard parton-parton scattering. New data on inclusive cross sections of jet production in $p + p$ collisions at the LHC [85–88] were analysed in the framework of z-scaling [29, 30]. We used the parameter values $c = 1$, $\delta = 1$, $\epsilon_{jet} = 0$, and $m_a = m_b = 0$ for the analysis. The results are compared with z-presentation of jet spectra in $\bar{p} + p$ collisions at the Tevatron [89–93, 96–102].

3.5.1. Angular independence. Figure 5 shows the inclusive spectra [89] of jet production in $\bar{p} + p$ collisions at the energy $\sqrt{s} = 1960$ GeV over the transverse momentum $p_T = 50$–600 GeV/c and pseudorapidity $|\eta| < 2.4$ ranges in p_T (a) and z (b) presentation. The experimental data collected by the DØ Collaboration correspond to the integrated luminosity of 0.7 fb^{-1}. As seen from Fig. 5a, the spectra measured for different pseudorapidity intervals demonstrate strong angular dependence. The difference in the behavior of the cross sections is enhanced with the increasing transverse momentum. The jet yields decrease with p_T in the measured momentum range more than ten orders of magnitude. Figure 5b demonstrates the angular independence of $\psi(z)$ over a wide kinematic range. The scaling function is described by a power law, $\psi(z) \sim z^{-\beta}$, with constant value of the slope parameter β.

The angular dependence of the transverse momentum spectra of jet production in $\bar{p} + p$ collisions was studied experimentally by the CDF Collaboration [90–93]. The differential cross sections obtained at $\sqrt{s} = 1960$ GeV are shown in Fig. 6a. The data cover the pseudorapidity range $|\eta| < 2.1$. The highest measured transverse energy carried by one jet was about 600 GeV. As seen from Fig. 6a, the transverse momentum spectra demonstrate strong dependence on the pseudorapidity of the produced jet. The z-presentation of the same data is shown in Fig. 6b. Points correspond to the mean values of the transverse momentum in the respective p_T bins. The data demonstrate angular independence and power behavior of the scaling function $\psi(z)$ over the range $z \simeq (0.15$–$10) \times 10^3$. We would like to emphasize that this result is a new confirmation of the properties of the z-scaling (energy and angular independence of $\psi(z)$) found at lower energy [29, 30]. The comparison concerns the inclusive jet production measured by the STAR Collaboration in $p + p$ collisions at $\sqrt{s} = 200$ GeV at RHIC, as well as other data on jet cross sections from FNAL and ISR.

Based on the performed study we conclude that the Tevatron data on jet production measured by the CDF and DØ Collaborations in Run II confirm z-scaling. The obtained results mean that the interactions of the constituents, their substructure and mechanism of jet

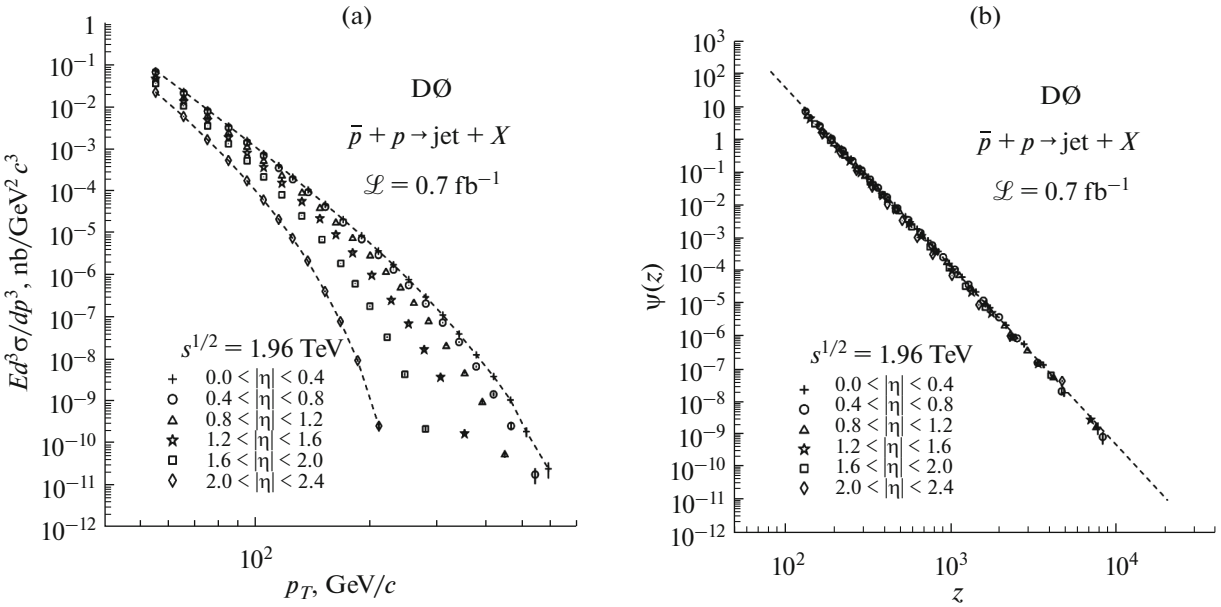

Fig. 5. The inclusive spectra of jet production in $\bar{p} + p$ collisions measured at $\sqrt{s} = 1960$ GeV and different pseudorapidity intervals presented in p_T (a) and z (b) presentation. Experimental data obtained by the DØ Collaboration are taken from [89, 100].

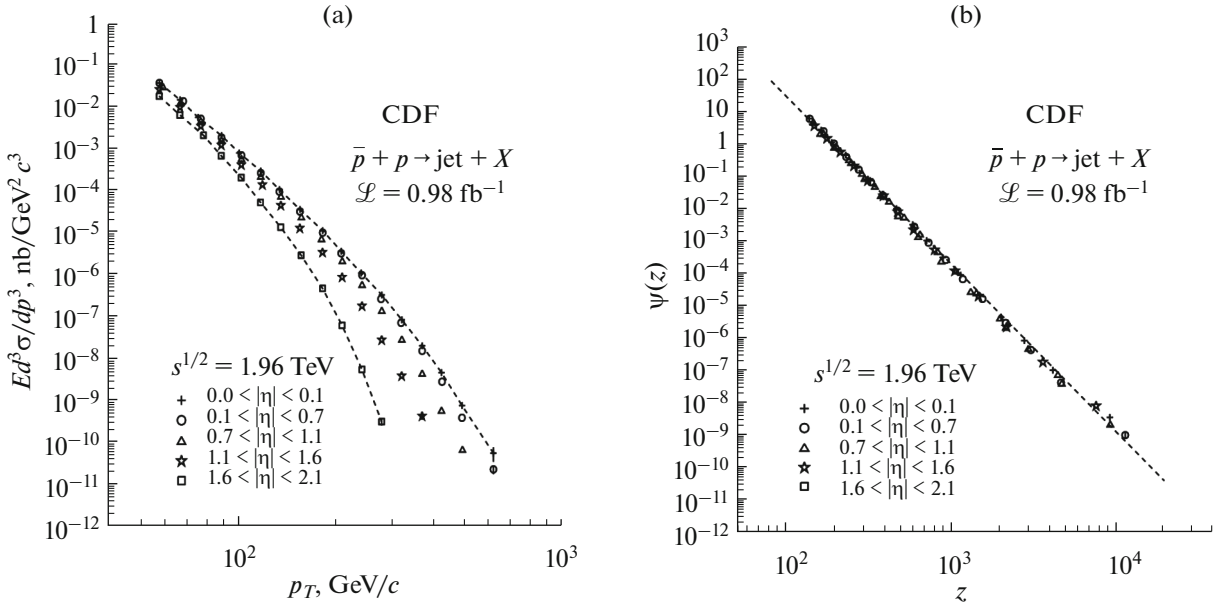

Fig. 6. The inclusive spectra of jet production in $\bar{p} + p$ collisions measured at $\sqrt{s} = 1960$ GeV and different pseudorapidity intervals presented in p_T (a) and z (b) presentation. Experimental data obtained by the CDF Collaboration are taken from [90–93].

formation reveal properties of self-similarity over a wide scale range (down to 10^{-4} fm).

New data on inclusive production of jets at the LHC allow us to verify the properties of z-scaling in the multi-TeV energy region. Here we report on study of z-presentation of the jet transverse momentum distributions measured by the CMS [87] and ATLAS [88] Collaborations in $p + p$ collisions at $\sqrt{s} = 8$ TeV. The obtained results are compared with data on jet production in $\bar{p} + p$ collisions at the Tevatron [89, 93]. Figure 7 demonstrates the p_T (a) and z (b) presentation of the jet spectra at $\sqrt{s} = 8$ TeV obtained by the CMS Collaboration in various pseudorapidity intervals [87]. Figure 8 shows the p_T (a) and z (b) presentation of the jet spectra at $\sqrt{s} = 8$ TeV obtained by the ATLAS Collaboration in various pseudorapidity inter-

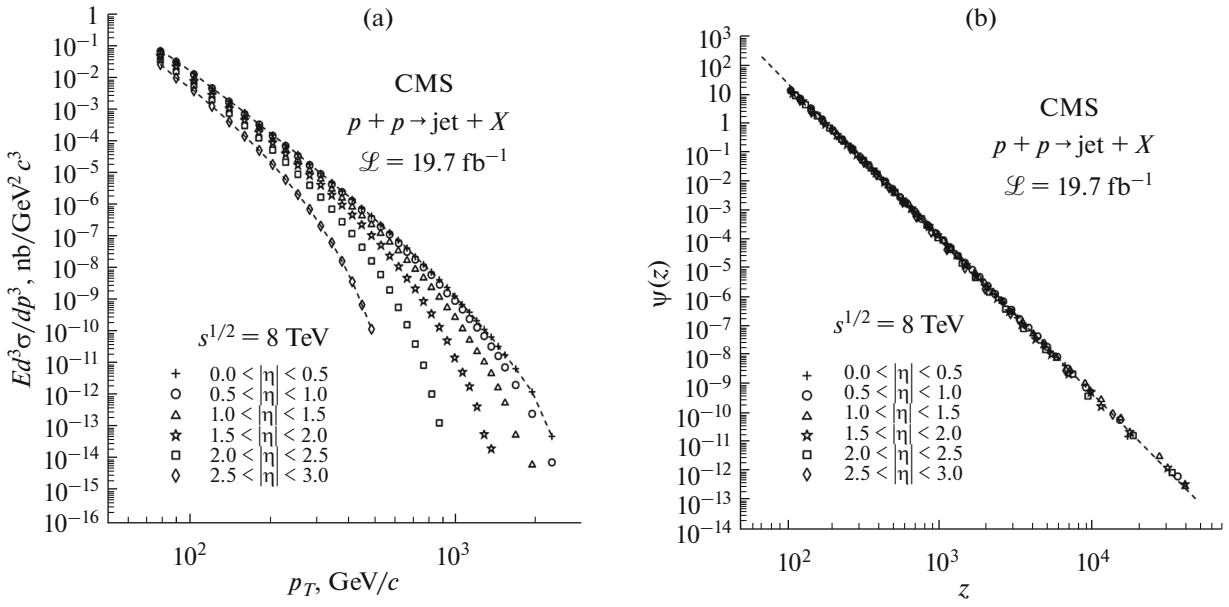

Fig. 7. The inclusive spectra of jet production in $p + p$ collisions measured at $\sqrt{s} = 8$ TeV and different pseudo-rapidity intervals presented in p_T (a) and z (b) presentation. Experimental data obtained by the CMS Collaboration are taken from [87].

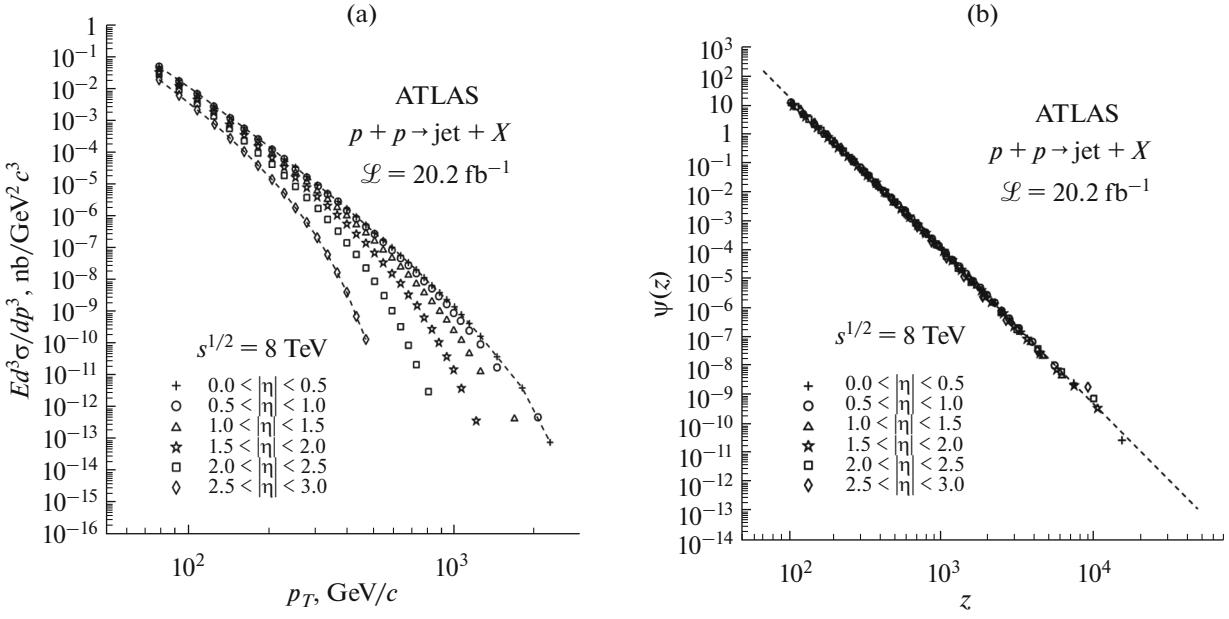

Fig. 8. The inclusive spectra of jet production in $p + p$ collisions measured at $\sqrt{s} = 8$ TeV and different pseudorapidity intervals presented in p_T (a) and z (b) presentation. Experimental data obtained by the ATLAS Collaboration are taken from [88].

vals [88]. One can see from Figs. 7b and 8b that the LHC measurements support the angular independence of the z-scaling for jet production in the new energy domain. The power behavior of the scaling function $\psi(z)$ at high z is also confirmed.

As follows from Figs. 5–8, the combined analysis of the data on jet production from the DØ, CDF, CMS, and ATLAS Collaborations manifests the angular independence of the scaling function $\psi(z)$.

3.5.2. Energy independence. We analyzed LHC data on inclusive cross sections of jets produced in $p + p$ collisions at $\sqrt{s} = 2.76$, 7, and 8 TeV in the z-scaling scheme. The obtained results are compared with the z-presentation of jet spectra obtained at the Teva-

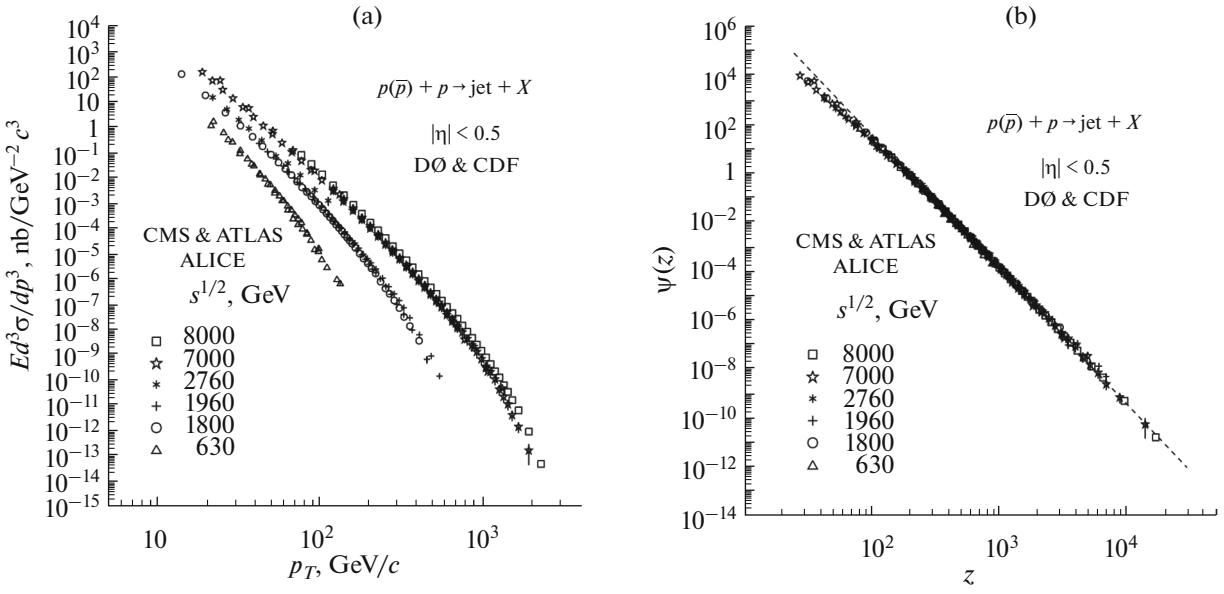

Fig. 9. The inclusive spectra of jet production in $p + p$ and $\bar{p} + p$ collisions in p_T (a) and z (b) presentation measured at $\theta \simeq 90°$. The symbols denote the ATLAS [85, 88, 95], CMS [87, 94], and ALICE [86] data obtained in $p + p$ collisions at $\sqrt{s}$ = 2760, 7000, 8000 GeV, and the DØ [89, 96–100] and CDF [90–93, 101, 102] data obtained in $\bar{p} + p$ collisions at $\sqrt{s}$ = 630, 1800, 1960 GeV, respectively.

tron in $\bar{p} + p$ collisions at the energies $\sqrt{s}$ = 630, 1800, 1960 GeV.

Figure 9a shows p_T-dependence of jet spectra measured in the central pseudorapidity window $|\eta| < 0.5$ by the CMS [87, 94], ATLAS [85, 88, 95], and ALICE [86] Collaborations at the LHC and the spectra obtained in the mid-rapidity region by the DØ [89, 96–100] and CDF [90–93, 101, 102] Collaborations at the Tevatron. The data collected by the CMS Collaboration correspond to the integrated luminosity of 19.7 fb^{-1}. The spectra were measured up to the transverse momentum p_T = 2500 GeV/c. The ATLAS data cover the range $20 < p_T < 2500$ GeV/c. Both data reveal angular independence of the z-scaling (see Figs. 7, 8).

Figure 9b demonstrates z-presentation of the jet spectra shown in Fig. 9a. The energy independence of $\psi(z)$ for jet production and its power behavior over the range $\sqrt{s}$ = 630–8000 GeV at $\eta \simeq 0$ are confirmed. The scaling function changes more than twelve orders of magnitude and can be described by a power law, $\psi(z) \sim z^{-\beta}$, over a wide z-range. The dashed line in Fig. 9b corresponds to the asymptotic behavior of $\psi(z)$. The data obtained at the LHC confirm results of the analysis [29, 30] of jet spectra measured by the DØ and CDF Collaborations in $\bar{p} + p$ collisions at the Tevatron with parameters $\delta = 1$ and $c = 1$.

The comparison of the LHC and Tevatron data on jet production confirms energy and angular independence of the z-scaling and indicates on the universality of the shape of the scaling function in $p + p$ and $p + \bar{p}$ collisions.

4. SCALING FEATURES IN NUCLEAR COLLISIONS AT RHIC

Experimental results from RHIC and LHC support the hypothesis that a new state of nuclear matter is created in the collisions of heavy ions at high energy. The created matter with partonic degrees of freedom, the Quark–Gluon Plasma, reveals features of a strongly-coupled medium. Among the properties of the new medium there is opacity characterized by the suppression of particle yields and viscosity which is found to be such small that the matter looks like an ideal liquid rather than a gas of free quarks and gluons. It is assumed that the medium produced in heavy-ion collisions is thermalized. Therefore the yields of most of the produced particles get fixed at chemical freeze-out. The statistical thermal models have successfully described the chemical freeze-out stage with unique system parameters such as chemical freeze-out temperature $T_{\rm ch}$ and baryon chemical potential μ_B [103–107]. The phase diagram of nuclear matter is usually presented in the temperature-baryon chemical potential plane $\{T, \mu_B\}$. Both quantities can be varied by changing the energy and centrality of the nuclear collisions and the type and momentum of the produced particles. The phase diagram should demonstrate a possible transition from a high energy density and high temperature

phase in which quark and gluon degrees of freedom dominate to a phase where the relevant degrees of freedom are hadronic [48, 108–112].

The idea of the BES programs at RHIC is to scan the QCD phase diagram from the top RHIC energy to the lowest possible energy achievable at this collider [108]. The program is aimed to perform systematic investigation and data analysis of particle production in the heavy-ion interactions over a wide range of collision energy and centrality. It includes spectra of identified hadrons, multiplicity densities, average transverse momenta, particle ratios and others. The systematic measurements performed with heavy-ions are of great interest to search for critical phenomena in a broad range of kinematic variables.

In the collisions of heavy nuclei, the phase transitions and other collective effects must show up in a larger space volume than in proton-proton collisions. It is expected that they may result in a change of properties of particles themselves and could influence the interaction mechanisms of hadron constituents as well as fragmentation processes by their production. The modification of the latter is due to the specific properties of the nuclear medium (high energy density and temperature of the medium).

In order to study changes and modifications in the nuclear interactions at a constituent level, we extend the applicability of the self-similarity principle to description of hadron production in nucleus-nucleus collisions. We expect that this important physical principle should be valid in the high-density and high-temperature phase in which quark and gluon degrees of freedom dominate, and also in the phase where the relevant degrees of freedom are hadronic. The self-similarity concerns fractal structure of the colliding objects, interaction of their constituents and fractal character of fragmentation processes in the final state. Based on the self-similarity arguments one can search for changes of the z-scaling parameters in the nuclear system relative to ones established in $p + p$ interactions. A discontinuity or abrupt change of the model parameters—the fractal and fragmentation dimensions and "specific heat"—may indicate to a signature of a phase transition or a critical point in the matter produced in nuclei collisions.

4.1. Modification of Model Parameters in A + A Collisions

The STAR heavy-ion results obtained in the RHIC BES-I program were presented in [48, 109–112]. The experimental data obtained from Au + Au interactions at $\sqrt{s_{NN}} = 7.7$, 11.5, 19.6, 27, and 39 GeV contain valuable information in the energy region which is subject of intense study. The transverse momentum spectra of hadrons produced in the high energy collisions of heavy ions reflect features of constituent interactions in nuclear medium. The medium modification processes (recombination, coalescence, energy loss, multiple scattering, ...) affect the shape of the measured p_T-distributions. Their influence on the spectra was experimentally regulated by variation of the event centrality and collision energy. The assumption of self-similarity, manifested by the z-scaling in proton-proton interactions, is applied to the nucleus-nucleus collisions as well. It was shown [33] that spectra of charged particles for different centrality classes in $A + A$ collisions characterized by different multiplicity densities exhibit similar scaling behavior as observed in $p + p$ collisions. It was also demonstrated [39] that spectra of pions indicate similarity as a characteristic feature of the mechanism of pion production in $A + A$ collisions at RHIC energies. These results encourage us to use the z-scaling approach for analysis of the spectra of negative hadrons measured by the STAR Collaboration in the BES-I program at RHIC.

We found that z-presentation of the spectra of negative hadrons in peripheral Au + Au collisions and in $p + p$ interactions coincide with each other with good accuracy when using $c_{\mathrm{AuAu}} = 0.11$. Moreover, this value is consistent with energy independence of $\psi(z)$ in the peripheral Au + Au collisions. It indicates that the form of the spectra in peripheral collisions is in a sense insensitive to modifications of the production mechanism by nuclear medium when compared with $p + p$ data. The influence of nuclei is included with a drop-off in the "specific heat" from its value $c_{pp} = 0.25$ in $p + p$ collisions to the value of $c_{\mathrm{AuAu}} = 0.11$ for the Au + Au interactions. The decrease of the specific heat can be understood by a relative diminishing of the average compactness of the $A + A$ system relative to the $p + p$ one.

We observed that the same scaling behavior as for $p + p$ collisions can be obtained for Au + Au interactions for all centralities. It can be achieved by the parameter ϵ_{AA} allowing it to be a function of the multiplicity density. For that purpose we used the linear parametrization

$$\epsilon_{AA} = \epsilon_0 (2N_{\mathrm{neg}}^{AA} / d\eta|_0) + \epsilon_{pp}, \qquad (9)$$

with a suitable choice of ϵ_0. The increase of ϵ_{AA} with multiplicity density is connected with a decrease of the momentum fractions y_a and y_b. It results in larger energy losses in final state for large centralities (multiplicities). The energy losses depend on the traversed medium which converts them into the multiplicity of the produced particles. This leads to the fact that the more produced multiplicity $N_{\mathrm{ch}}^{AA} \simeq 2N_{\mathrm{neg}}^{AA}$ per unit of (pseudo)rapidity, the larger energy loss of the secondary particles. The multiplicity density characterizes the produced medium and is connected in this way to the energy losses in the medium.

4.2. Negative Hadron Production in Au + Au *Collisions*

The spectra of negatively charged hadrons measured by the STAR Collaboration in Au + Au collisions at $\sqrt{s_{NN}}$ = 7.7, 11.5, 19.6, 27, 39, 62.4, and 200 GeV at mid-rapidity $|\eta| < 0.5$ as a function of the transverse momentum p_T for different centrality classes of (0–5), (5–10), (10–20), (20–40), (40–60), (60–80)% are presented in [46]. The distributions were obtained over a wide momentum range $0.2 < p_T < 12$ GeV/c. It was found that the spectra exhibit exponential and power behavior in dependence on p_T at $\sqrt{s_{NN}}$ = 7.7 and 200 GeV, respectively. The spectra for the most central and peripheral collisions reveal strong sensitivity on $\sqrt{s_{NN}}$, especially in the high-p_T region. The difference between the yields of the negative hadrons at $\sqrt{s_{NN}}$ = 7.7 and 200 GeV is more than two orders of magnitudes at p_T = 4 GeV/c.

4.2.1. Centrality(multiplicity) dependence. The fractal dimension ϵ_{AA} characterizing fragmentation of objects produced directly in the constituent collisions is suggested to be a function of multiplicity density in the nuclear medium. The multiplicity density $dN^{AA}_{\rm neg}/d\eta\big|_0$ of negative particles in the central interaction region ($\eta = 0$) depends on the centrality selection criteria of nuclear collisions. The value of the multiplicity density in the central collisions is about 6 times larger than for the peripheral ones. The density changes from 16 to 96 at $\sqrt{s_{NN}}$ = 7.7 GeV and from 50 to about 250 at $\sqrt{s_{NN}}$ = 200 GeV. The growth of $dN^{AA}_{\rm neg}/d\eta\big|_0$ with centrality results in a considerable increase of ϵ_{AA} and thus in larger energy losses by production of the inclusive particles. The effect becomes more significant at higher energy as both the multiplicity density and the parameter ϵ_0 increase with $\sqrt{s_{NN}}$. The multiplicity density of negative particles in Au + Au collisions is considered to regulate the energy density of the produced medium. Due to the high energy density and temperature of the produced matter, the most central events are expected to be preferable to search for signatures of a phase transition and a critical point. Let us illustrate centrality dependence of some scaling features of hadron interaction at constituent level using the z-presentation of inclusive spectra of negative particles produced in Au + Au collisions at two energies, $\sqrt{s_{NN}}$ = 27 and $\sqrt{s_{NN}}$ = 200 GeV.

Figure 10a shows the dependence of the function $\psi(z)$ on the variable z for the negative hadrons [46] produced in Au + Au collisions at the energy $\sqrt{s_{NN}}$ = 27 GeV for different centralities. One can see a "collapse" of the z-presentation of the data points onto a single curve. The solid line corresponds to the z-scaling of inclusive hadrons established in $p + p$ collisions. The centrality independence of $\psi(z)$ for the Au + Au system reveals approximately the same scaling behavior as shown by the proton–proton reference curve. This together with the energy, angular and multiplicity independence of the scaling function gives strong constraint on the values of the model parameters. The parameter c interpreted as a "specific heat" of the bulk of the produced matter is found to be constant, independent on energy and centrality of collisions. Its value $c_{\rm AuAu} = 0.11$ is consistent with the scaling behavior for all analyzed centralities and energies (see also Fig. 11). Note that the "specific heat" corresponding to the z-scaling in $p + p$ interactions is about $c_{pp} = 0.25$. In accordance with the additive property of fractal dimensions of nuclei observed in $p + A$ systems, we used $\delta_A = A\delta$ with the same value of $\delta = 0.5$ as for $p + p$ data. The fractal dimension $\delta_{\rm Au}$ of the colliding nuclei is found to be independent on the collision centrality. For the RHIC energies $\sqrt{s_{NN}} \gtrsim 19$ GeV, the dimension $\delta_{\rm Au}$ does not depend on energy either. The fragmentation dimension ϵ_{AA} of the fragmentation processes is assumed to be a function (9) of the multiplicity density and thus depends on the centrality of nuclear collisions. We have found that $\epsilon_{\rm AuAu}$ is an increasing function of the collision centrality with $\epsilon_0 = 0.0012$ at $\sqrt{s_{NN}}$ = 27 GeV. The value of $\epsilon_{pp} = 0.2$ is energy independent. It was found from the z-scaling in $p + p$ interactions.

Figure 10b shows the dependence of the fraction Ax_1 on the transverse momentum of negative hadrons produced in Au + Au collisions at $\sqrt{s_{NN}}$ = 27 GeV for different centralities. The momentum fractions Ax_1 and Ax_2 determine the total energy of the constituent sub-process which underlies production of the inclusive particle with a given p_T. In the considered case of the symmetric kinematics of the produced particles both fractions are equal each other. One can see from Fig. 10b that the fraction Ax_1 increases with transverse momentum. For a fixed p_T, the values of Ax_1 become larger for the collisions with larger centralities, whereas x_1 takes the smallest value for $p + p$ interactions. Let us estimate energy of the underlying constituent sub-process in the $p + p$ system and compare it with the energies of the constituent sub-processes in 40–60% peripheral and 0–5% central Au + Au events. At p_T = 1 GeV/c, the corresponding momentum fractions $Ax_1 (= Ax_2)$ are approximately equal to 0.18, 0.22, and 0.31, which gives the following energies $\sqrt{s_x}$ = 4.9, 5.9, and 8.4 GeV of the constituent collisions. At higher momentum, say p_T = 6 GeV/c, the corresponding values of Ax_1 are about 0.53, 0.66, and 0.83, which results in $\sqrt{s_x}$ = 14, 18, and 22 GeV, respectively. These estimates illustrate how the energy

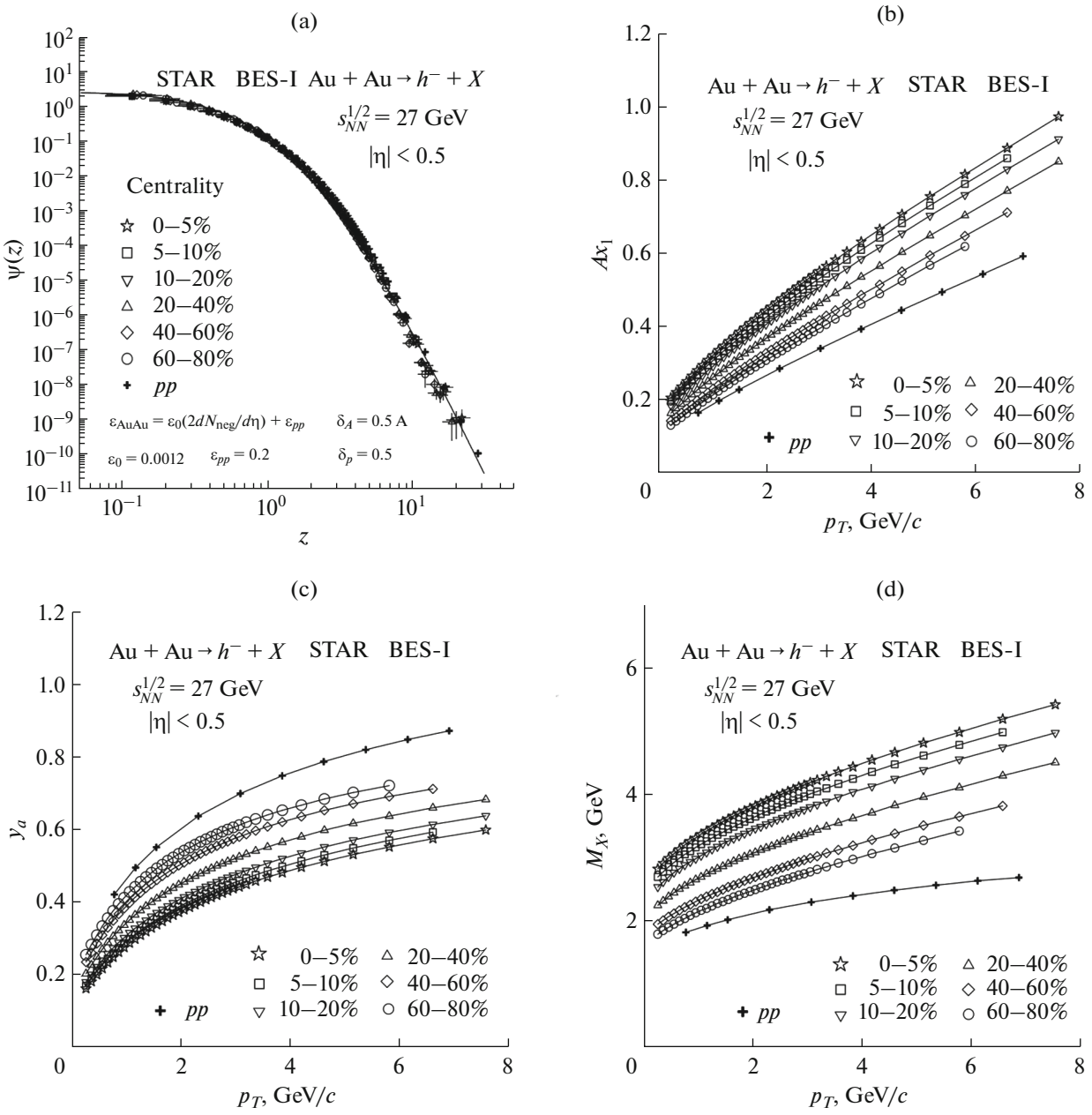

Fig. 10. Scaling function $\psi(z)$ (a), momentum fractions x_1 (b), y_a (c), and recoil mass M_X (d) for negative hadrons produced in Au + Au collisions at $\sqrt{s_{NN}}$ = 27 GeV and different centralities as a function of transverse momentum p_T. The symbols correspond to the experimental data [46] measured by the STAR Collaboration at RHIC. The error bars shown are statistical only.

consumption in the constituent interaction increases with transverse momentum and how it becomes larger when going from the $p + p$ collisions to the Au + Au collisions with different centralities. The inclusive production of a negative hadron with the same transverse momentum needs more energy in the constituent sub-process due to the created medium in the nuclear system than in the proton-proton one. With the increasing collision centrality, the created medium becomes more dense and the energy of the constituent interaction must be even larger. The corresponding enhanced energy consumption is a consequence of the larger energy losses by fragmentation processes and larger recoil mass in constituent sub-processes in the central collisions of heavy nuclei that are considerably larger than in the peripheral nuclear collisions and also in the $p + p$ interaction. This property is demonstrated in the next.

The quantities which characterize the process with energy loss in the z-scaling scheme are the fractal

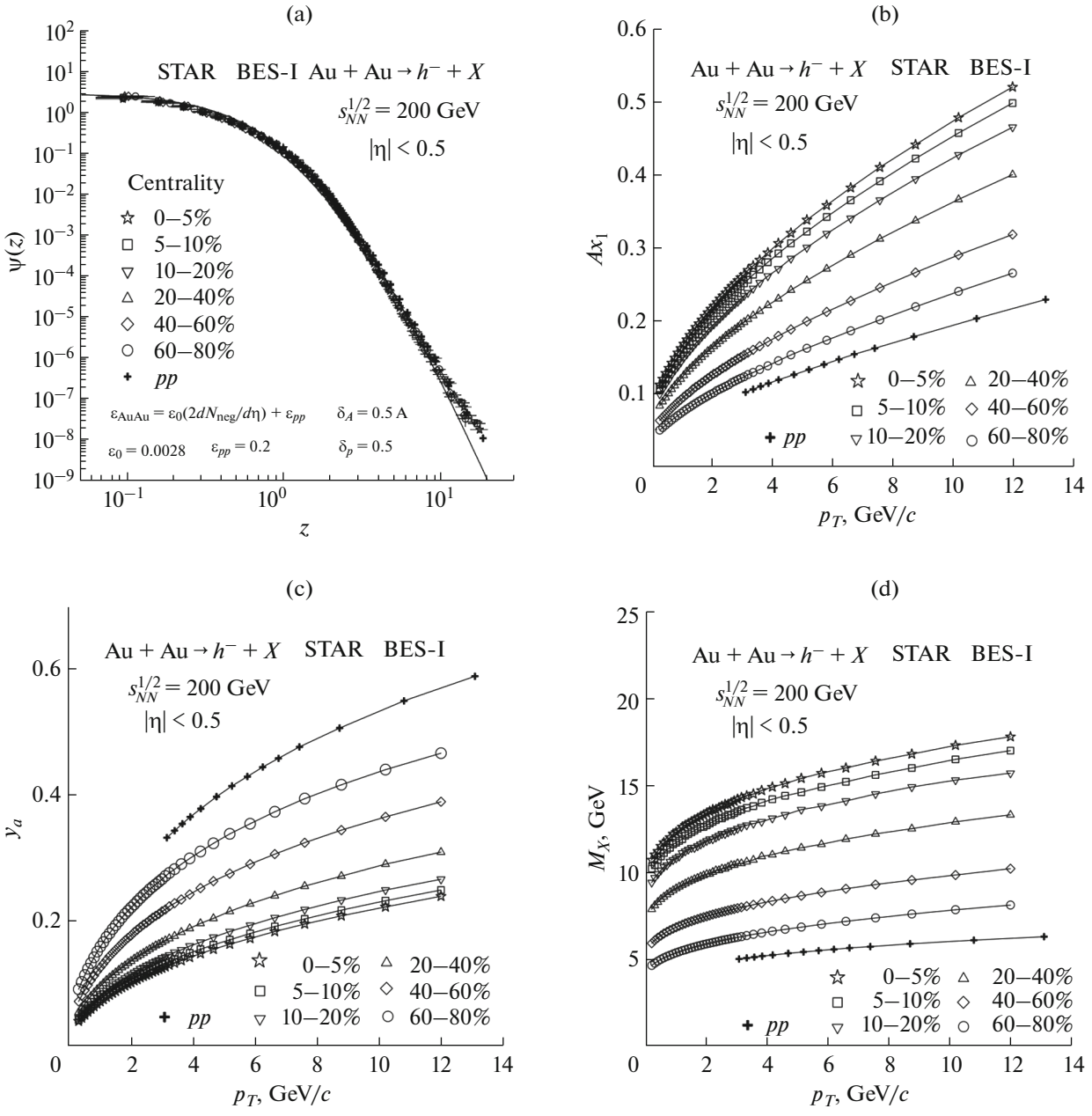

Fig. 11. Scaling function ψ(z) (a), momentum fractions x_1 (b), y_a (c), and recoil mass M_X (d) for negative hadrons produced in Au + Au collisions at $\sqrt{s_{NN}}$ = 200 GeV and different centralities as a function of transverse momentum p_T. The symbols correspond to the experimental data [46] measured by the STAR Collaboration at RHIC. The error bars shown are statistical only.

dimension ε_{AA} and the momentum fraction y_a. The relative energy loss of the scattered constituent with energy E_q is given by the relation $\Delta E_q / E_q = (1 - y_a)$. Its dependence on the transverse momentum of the inclusive hadron gives information on the medium created in the collisions of heavy nuclei and also on the fragmentation properties of particles produced in the constituent collisions. Figure 10c shows the dependence of the fraction y_a on the transverse momentum p_T of negative hadrons produced in Au + Au collisions at $\sqrt{s_{NN}}$ = 27 GeV for different centralities. The values of y_a for $p + p$ collisions at the same energy are shown by the crosses. As seen from the figure, the fraction y_a increases with hadron's transverse momentum and decreases with the collision centrality. To get a quantitative idea, let us consider the energy loss in the $p + p$ system and compare it with the energy losses in 40–60% peripheral and 0–5% central Au + Au

events. At $p_T = 1$ GeV/c, the corresponding momentum fraction y_a is approximatively equal to 0.48, 0.40, and 0.30. From the estimated 52, 60, and 70% relative energy losses one obtains the absolute energy dissipations when using the relation $\Delta E_q/E_q = (1 - E_p/E_q)$ with $E_p \simeq p_T$. The absolute energy losses are $\Delta E_q =$ 1.1, 1.5, and 2.3 GeV, in $p + p$, 40–60% Au + Au peripheral, and 0–5% central Au + Au collisions at this low p_T, respectively. At higher $p_T = 6$ GeV/c, the corresponding values of y_a are about 0.82, 0.69, and 0.55. The relative energy losses are 18, 31, and 45%, while the absolute energy dissipations are $\Delta E_q = 1.6$, 2.7, and 4.9 GeV, respectively. These estimates illustrate how the energy released in the fragmentation process depends on the transverse momentum of the inclusive negative hadron. While the relative energy loss decreases with the increasing p_T, the absolute energy dissipation behaves in the opposite way. The values of ΔE_q become larger for the higher transverse momentum in all considered colliding systems. On the other hand the energy loss, relative and absolute, increases when going from the $p + p$ interaction to the peripheral and central Au + Au collisions at both considered p_T. The inclusive production of a negative hadron with the same transverse momentum is characterized with more energy loss due to the created medium in the nuclear system than in the proton–proton one. With the increasing collision centrality, the created medium becomes more dense and the energy dissipation must be even larger. Let us note however that at fixed centrality, the larger values y_a correspond to smaller relative energy losses which give better conditions to reveal a phase transition or vicinity of a critical point.

Figure 10d shows the dependence of the recoil mass $M_X = x_1 M_1 + x_2 M_2 + m_b/y_b$ on transverse momentum of negative hadrons produced at the energy $\sqrt{s_{NN}} = 27$ GeV in Au + Au collisions for different centralities. The recoil mass increases with the transverse momentum p_T of the inclusive hadron and also with the collision centrality. The values of M_X for $p + p$ collisions at the same energy are shown by the crosses. At $p_T = 1$ GeV/c, the recoil mass is equal to $M_X = 1.8$, 2.3, and 3.3 GeV for the $p + p$, 40–60% peripheral and 0–5% central Au + Au collisions, respectively. This difference increases with transverse momentum and at $p_T = 6$ GeV/c the values of the recoil mass are $M_X = 2.6$, 3.7, and 5.0 GeV, respectively. The p_T-dependence of the recoil mass is influenced mainly by the momentum fraction y_b which is much smaller than y_a. Relatively small values of y_b mean that the momentum balance in the production of an inclusive particle is more likely compensated by many particles with smaller momenta than by a single particle with higher momentum moving in the opposite direction.

The properties of $\psi(z)$, Ax_1, y_a, M_X and their dependencies on the centrality of Au + Au collisions at the energy $\sqrt{s_{NN}} = 200$ GeV are illustrated in Fig. 11. Let us compare these properties with the similar features found at the lower energy $\sqrt{s_{NN}} = 27$ GeV. Figure 11a demonstrates independence of the scaling function $\psi(z)$ on the collision centrality. A "collapse" of the z-presentation of data points on a single curve is clearly seen. The solid line is a reference representing the z-scaling of inclusive hadrons in $p + p$ interaction. The centrality independence of $\psi(z)$ for the gold-gold system was obtained under the following conditions. The same value, $c_{\mathrm{AuAu}} = 0.11$, was assigned to the parameter interpreted as a "specific heat" for all centralities as used at the energy $\sqrt{s_{NN}} = 27$ GeV. For the fractal dimension of nucleus with the atomic number A we set $\delta_A = A\delta$, where $\delta = 0.5$ is the nucleon fractal dimension found from $p + p$ data. The relation (9) was exploited to express the centrality dependence of the fragmentation dimension ϵ_{AuAu} with $\epsilon_0 = 0.0028$ at $\sqrt{s_{NN}} = 200$ GeV. The value of $\epsilon_{pp} = 0.2$ was fixed. We used the multiplicity density of negative particles produced in Au + Au collisions at different centralities in relation (6). In the formula (5) we set $N_{\mathrm{ch}}^{AA}/d\eta\big|_0 \simeq 2N_{\mathrm{neg}}^{AA}/d\eta\big|_0$. The parameters allow us to describe the function $\psi(z)$ by the same curve in $p + p$ interaction and in Au + Au collisions at all centralities except few points at the end of the spectra at $\sqrt{s_{NN}} = 200$ GeV. The discrepancy of $\psi(z)$ at this energy needs further investigation. A verification of the power law, $\psi \sim z^{-\beta}$, in the asymptotic region ($z > 20$) is of interest to search for new constituent properties and mechanisms of their interaction in the collisions of heavy nuclei.

Results presented in Fig. 11b demonstrate smooth dependence of the fraction Ax_1 on the transverse momentum of negative hadrons produced at $\sqrt{s_{NN}} = 200$ GeV and support the properties found at the energy $\sqrt{s_{NN}} = 27$ GeV. The fraction Ax_1 increases with collision centrality and the transverse momentum p_T. As follows from Fig. 11b, the energies of the constituent sub-processes are higher than at $\sqrt{s_{NN}} =$ 27 GeV. In order to make a quantitative feeling we estimate the energy of the underlying sub-process in the $p + p$ interaction, 40–60% peripheral and 0–5% central Au + Au collisions at the same transverse momentum $p_T = 6$ GeV/c as for the lower collision energy. The corresponding momentum fractions $Ax_1 (= Ax_2)$ are approximately equal to 0.14, 0.21, and 0.35, which gives the following energies $\sqrt{s_x} = 28$, 42,

and 70 GeV of the constituent collisions. At higher momentum $p_T = 12$ GeV/c, the momentum fractions are about 0.22, 0.32, and 0.52, giving $\sqrt{s_x} = 44$, 64, and 104 GeV, respectively. The difference between the fractions in the $p + p$ interaction and in the Au + Au collisions increases with p_T and is significantly larger than at the smaller energy $\sqrt{s_{NN}} = 27$ GeV. The corresponding enhanced energy consumption is a consequence of the larger energy losses by fragmentation processes and the larger recoil mass in constituent sub-processes at higher $\sqrt{s}$ and in the central collisions of heavy nuclei, as demonstrated in the following.

Figure 11c shows the dependence of the momentum fraction y_a on the transverse momentum p_T of negative hadrons produced at $\sqrt{s_{NN}} = 200$ GeV for different centralities. The fraction y_a decreases with the collision centrality and increases with the transverse momentum of the inclusive particle. Let us estimate the energy loss by production of negative hadrons at this energy. We make a qualitative comparison of the energy loss in $p + p$ system with the energy losses in 40–60% peripheral and 0–5% central Au + Au collisions. At $p_T = 6$ GeV/c, the corresponding momentum fractions y_a are approximately equal to 0.43, 0.30, and 0.18. From the estimated 57, 70, and 82% relative energy losses one obtains the absolute energy dissipations when using the relation $\Delta E_q \simeq p_T(1 - y_a)/y_a$. The absolute energy losses by production of a negative hadron with $p_T = 6$ GeV/c are $\Delta E_q = 8$, 14, and 27 GeV, in $p + p$, 40–60% peripheral, and 0–5% central Au + Au collisions, respectively. At two times higher $p_T = 12$ GeV/c, the corresponding values of y_a are about 0.57, 0.39, and 0.23. At this high transverse momentum, the relative energy losses are 43, 61, and 77%, while the absolute energy dissipations amount to $\Delta E_q = 9$, 19, and 40 GeV, respectively.

When comparing with the estimates at lower collision energy, we can make the following conclusions: (1) While the relative energy loss decreases with the increasing transverse momentum, the absolute energy loss reveals an opposite trend in the considered p_T range. (2) The inclusive production of a negative hadron with the same p_T is accompanied with more energy loss due to the created medium in the nuclear system than in the proton-proton one. With the increasing collision centrality, the energy dissipation becomes larger because the produced medium becomes more dense. (3) The relative energy dissipation increases when going from the $p + p$ interaction to the peripheral and central nuclear collisions. The relative energy loss gets larger when the collision energy $\sqrt{s_{NN}}$ increases. (4) The ratio $\Delta E_q(200\text{ GeV})/\Delta E_q(27\text{ GeV})$ of the absolute energy losses at the two considered energies and $p_T = 6$ GeV/c is about 5.0, 5.2, and 5.5 in the $p + p$ interaction, 40–60% Au + Au peripheral, and 0–5% Au + Au central collisions, respectively. One can see that the largest increase of the absolute energy losses with the collision energy is in the central collisions of the gold nuclei. Note that the corresponding increase of $\sqrt{s_{NN}}$ is by the factor 7.4. Because the relative energy loss decreases with the transverse momentum and increases with the centrality and energy of the collisions, it is preferable to search for signatures of a phase transition in nuclear matter at high p_T, in a light nuclei system, and at middle collision energy.

Figure 11d shows the dependence of the recoil mass M_X on the transverse momentum p_T of negative hadrons produced in Au + Au collisions at $\sqrt{s_{NN}} = 200$ GeV for different centralities. The cross symbols depict the same quantity calculated at the same energy for the $p + p$ system. We observe a similar dependence of M_X on the collision centrality and transverse momentum of the inclusive hadrons as it was demonstrated at the lower energy $\sqrt{s_{NN}} = 27$ GeV. All curves reveal a characteristic growth with p_T. For larger transverse momenta in the $\sqrt{s_{NN}} = 200$ GeV gold system, the growth of the recoil mass is followed by a successive flattening. The values of M_X at $p_T = 6$ GeV/c are about 5.5, 8.5, and 16 GeV for the $p + p$, 40–60% peripheral and 0–5% central Au + Au collisions, respectively. The recoil mass increases with transverse momentum and at $p_T = 12$ GeV/c its values are approximately equal to $M_X = 6.5$, 10.2, and 18 GeV, respectively. A comparison of Figs. 10d and 11d shows that the sensitivity of the recoil mass to the centrality of nuclear collisions increases with $\sqrt{s_{NN}}$. From the observed results we conclude that the momentum balance in the production of an inclusive negative hadron is likely to be compensated by more particles at $\sqrt{s_{NN}} = 200$ GeV than at lower energies. The number of these particles moving in the direction opposite to the inclusive hadron increases rapidly with the energy and centrality of the gold collisions.

4.2.2. Peripheral collisions. Figure 12a shows the dependence of the function $\psi(z)$ on the variable z for negative hadrons [46] produced in the (40–60)% peripheral Au + Au collisions at different energies. The solid line is a fitting curve corresponding to the z-scaling of inclusive particles in $p + p$ interaction over the range $\sqrt{s} = 19$–200 GeV and $\theta_{\text{cms}} = 3°$–90°. One can see that the z-presentation of the spectra of negative hadrons produced in the peripheral gold collisions (shown by the symbols) and in the $p + p$ interactions (presented by the solid line) coincide with each other with good accuracy in the studied kinematic region. The energy independence of $\psi(z)$ for the Au + Au system was obtained by the same parameters

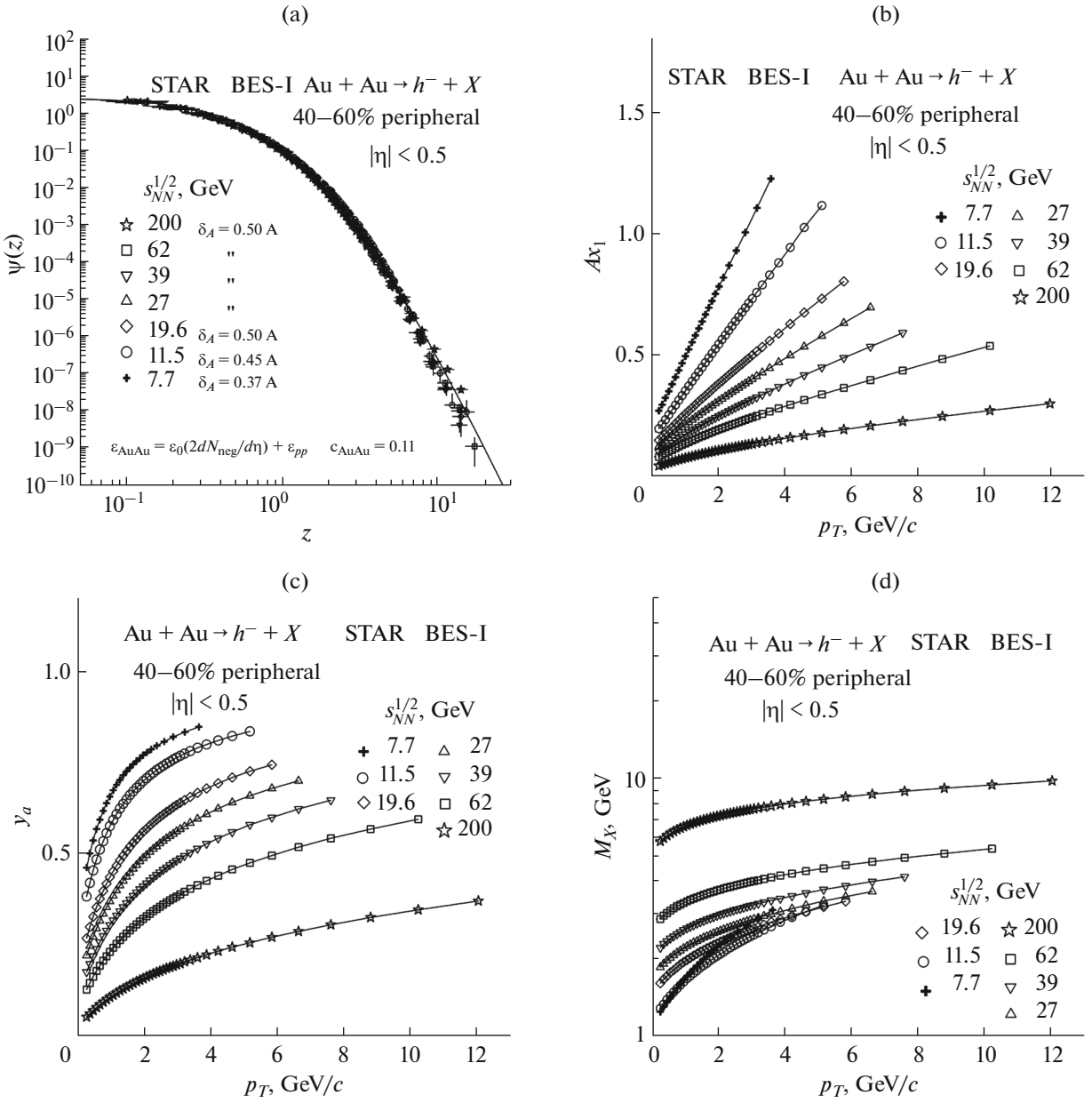

Fig. 12. Scaling function ψ(*z*) (a), momentum fractions x_1 (b), y_a (c), and recoil mass M_X (d) for negative hadrons produced in Au + Au collisions at $\sqrt{s_{NN}}$ = 7.7, 11.5, 19.6, 27, 39, 62.4, and 200 GeV for peripheral (40–60)% collisions as a function of transverse momentum p_T. The symbols correspond to the experimental data [46] measured by the STAR Collaboration at RHIC. The error bars shown are statistical only.

which give the multiplicity independence of the scaling function for different collision centralities. These properties, together with constancy of the fractal dimensions of the colliding nuclei in the region $\sqrt{s_{NN}} \gtrsim 19.6$ GeV, demonstrate universality of the z-presentation of inclusive spectra in various systems. For $\sqrt{s_{NN}} < 19.6$ GeV we found that the parameters δ_{Au}, δ_p, and ϵ_{pp} decrease with energy. This is a natural observation because the fractality of the interacting objects and fragmentation processes is expected to be smeared out at lower energies. In the limit of structureless objects, these parameters should be zero. Further observation is that the parameter c interpreted as specific heat of the bulk of the produced matter is found to be constant. The value of $c_{AuAu} = 0.11$ is consistent with the scaling behavior for all considered centralities and energies.

Figure 12b shows the fraction Ax_1 in dependence on the transverse momentum p_T for h^- hadrons produced in the 40–60% peripheral Au + Au collisions

for different collision energies. The momentum fractions x_1 and x_2 corresponding to the minimal resolution Ω^{-1} of the fractal measure z determine the energy of the underlying constituent sub-process. Both fractions x_1 and x_2 are equal to each other for particles detected at the angle $\theta_{cms} = 90°$ in the center-of-mass system of $p + p$ or $A + A$ interactions. Using the principle of the minimal resolution we determine the energy $\sqrt{s_x} = Ax\sqrt{s_{NN}}$ of the constituent sub-process which underlies production of the inclusive particle with the momentum p_T. Let us estimate the energy $\sqrt{s_x}$ in the 40–60% peripheral Au + Au collisions for the transverse momentum $p_T = 3$ GeV/c at the collision energies $\sqrt{s_{NN}} = 7.7$, 27, and 200 GeV. As can be seen from Fig. 12b, the corresponding momentum fractions $Ax_1 (= Ax_2)$ are about 1.07, 0.40, and 0.15. This results in the following energies $\sqrt{s_x} = 8.2$, $\sqrt{s_x} = 11$, and $\sqrt{s_x} = 30$ GeV of the underlying constituent interactions in the 40–60% peripheral Au + Au events at the considered energies, respectively. One can see that the energy of the constituent sub-processes increases when the collision energy becomes higher. The rate of the increase reflects the increase of the collision energy but also accounts for larger energy losses in fragmentation processes and larger recoil mass in the peripheral gold collisions at higher $\sqrt{s_{NN}}$.

Figure 12c depicts the momentum fraction y_a in dependence on the transverse momentum p_T of negative hadrons produced in the 40–60% peripheral Au + Au collisions at different energies. All curves demonstrate monotonic growth of y_a with p_T. Such a trend corresponds to ideas that the relative energy dissipation associated with a high-p_T particle is smaller when compared with the inclusive processes at lower transverse momenta. As seen from Fig. 12c, the relative energy loss $\Delta E_q / E_q = (1 - y_a)$ increases as the collision energy becomes higher. It is expressed by the diminishing of the fraction y_a with $\sqrt{s_{NN}}$ at constant values of transverse momenta. Let us estimate this effect at $p_T = 3$ GeV/c for the energies $\sqrt{s_{NN}} = 7.7$, 27, and 200 GeV. The corresponding values of the momentum fraction y_a are about 0.84, 0.58, and 0.22. For the relative energy dissipations one obtains 16, 42, and 78%, respectively. From the momentum fractions we estimate the absolute energy losses $\Delta E_q \simeq p_T(1 - y_a)/y_a$ in fragmentation processes by production of the negative hadrons with the momentum $p_T = 3$ GeV/c. Their values are about $\Delta E_q = 0.6$, 2.2, and 10.6 GeV at the energies $\sqrt{s_{NN}} = 7.7$, 27, and 200 GeV, respectively. One can see that both the relative and the absolute energy losses increase when the collision energy becomes higher. This is true also at the higher transverse momentum $p_T = 6$ GeV/c, where the relative energy dissipations amount to 31 and 71% resulting in $\Delta E_q = 2.7$ and $\Delta E_q = 14$ GeV at the energies $\sqrt{s_{NN}} = 27$ and 200 GeV, respectively. A comparison of the corresponding numbers at $p_T = 3$ and $p_T = 6$ GeV/c gives another property. Namely, while the relative energy losses decrease with the increasing transverse momentum, the absolute energy dissipations show the opposite trend in the considered region of p_T. The ratio $\Delta E_q (p_T = 6 \text{ GeV}/c)/\Delta E_q (p_T = 3 \text{ GeV})$ of the absolute energy losses at the two considered values of transverse momentum in the 40–60% peripheral Au + Au collisions is about 1.2 and 1.3 at the energies $\sqrt{s_{NN}} = 27$ and 200 GeV, respectively. One can see that, in peripheral gold–gold collisions, the increase of the absolute energy losses with p_T is only slightly larger at $\sqrt{s_{NN}} = 200$ GeV than at the lower energy $\sqrt{s_{NN}} = 27$ GeV.

Figure 12d shows the dependence of the recoil mass M_X on the transverse momentum p_T of negative hadrons produced in the 40–60% peripheral Au + Au collisions for different energies. All curves demonstrate an increase of the recoil mass with p_T. The growth of M_X with p_T and $\sqrt{s_{NN}}$ reflects evolution of the recoil sub-system in the medium created in nuclear collisions as its entropy increases. The values of the recoil mass correspond to the underlying constituent sub-process which is selected according to the principle of maximal entropy of the rest of the configurations at a constituent level. For a given p_T, the selection corresponds to the maximal entropy of the recoiling sub-system moving opposite to the inclusive particle. At $p_T = 3$ GeV/c, the value of M_X is about 2.9, 3.1, and 8 GeV, at the energy $\sqrt{s_{NN}} = 7.7$, 27, and 200 GeV, respectively. Let us note the relatively large value of M_X at the lowest energy $\sqrt{s_{NN}} = 7.7$ GeV. This anomaly corresponds to particle production in the cumulative region and is discussed in Sec. 4.2.4.

4.2.3. Central collisions. Figure 13a shows the dependence of $\psi(z)$ on the variable z for negative hadrons [46] produced in the most central 0–5% Au + Au collisions for different energies $\sqrt{s_{NN}}$. Important ingredient of the scaling is the fractal dimension of the fragmentation processes in the final state. For $p + p$ collisions, the fragmentation dimension ϵ_{pp} depends on the flavor content of the inclusive particles [47]. We expect therefore, that ϵ_{AA} in nuclear collisions will be different for different inclusive particles as well. For negative hadrons produced in $p + p$ collisions, the average fragmentation dimension is found to be constant $\epsilon_{pp} = 0.2$ at $\sqrt{s} \geq 19.6$ GeV. Based on the self-similarity considerations for the Au + Au system we

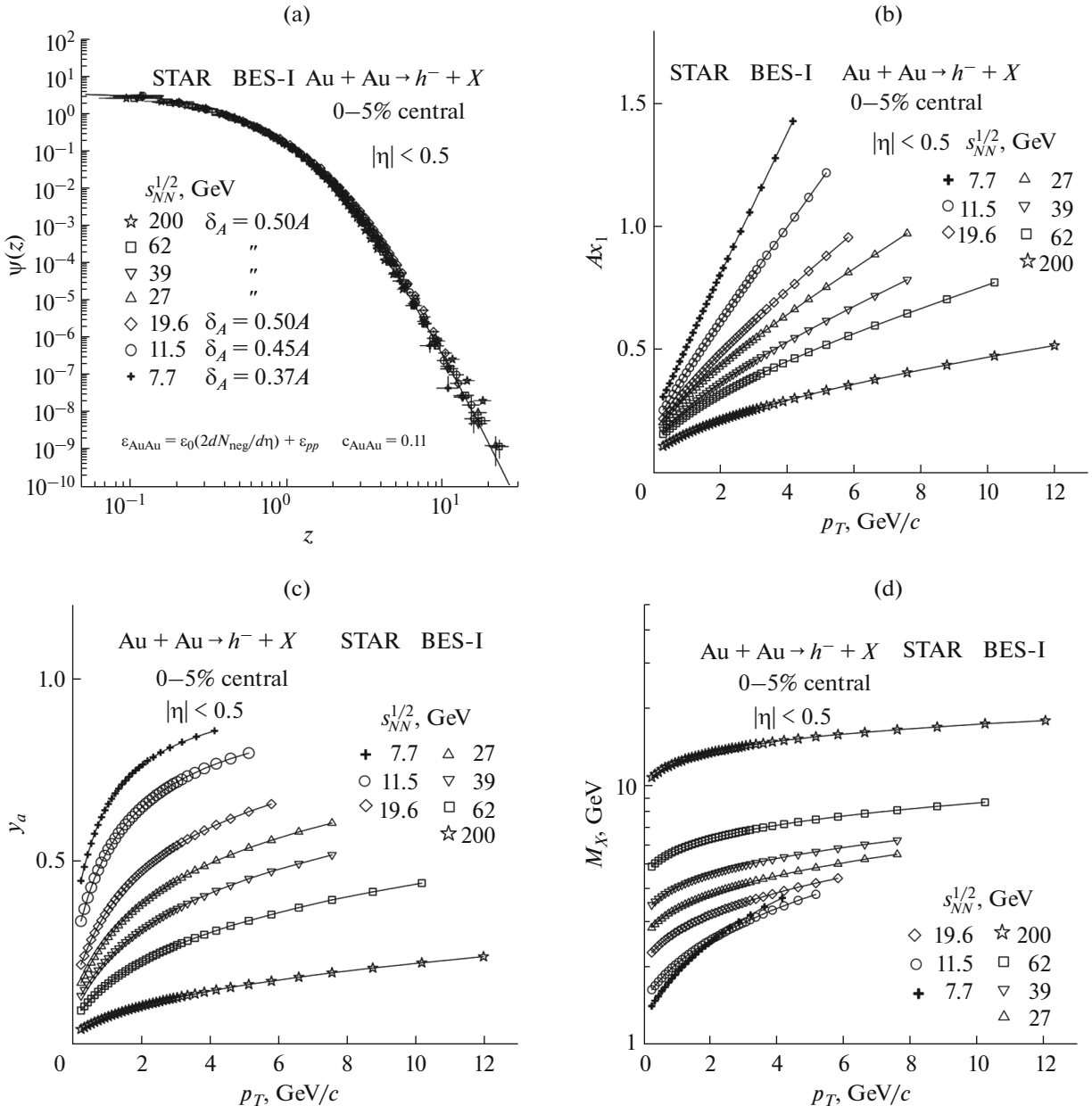

Fig. 13. Scaling function ψ(*z*) (a), momentum fractions x_1 (b), y_a (c), and recoil mass M_X (d) for negative hadrons produced in Au + Au collisions at $\sqrt{s_{NN}}$ = 7.7, 11.5, 19.6, 27, 39, 62.4, and 200 GeV for most central (0–5)% collisions as a function of transverse momentum p_T. The symbols correspond to the experimental data [46] measured by the STAR Collaboration at RHIC. The error bars shown are statistical only.

found that the corresponding fragmentation dimension ϵ_{AuAu} is an increasing function of the collision centrality (9). We expect such kind of dependence in the asymptotic region ($z > 20$) as well. The available data for non-identified hadrons allow us to perform reliable test of this assumption only partially.

The scaling behavior of negative particle production in Au + Au collisions was found in the environment with different multiplicity densities. The multiplicity scan of particle yields in nucleus-nucleus collisions at different energies gives complementary information on the production mechanisms in nuclear medium. The *z*-scaling can be interpreted as a result of a self-similar modification of elementary sub-processes by the created medium. We found no irregularities in the behavior of the scaling function ψ(*z*) over a wide range of $z = 0.1$–20. As seen from Fig. 13a, the errors of determination of the function ψ(*z*) at high *z*

are large. Nevertheless, indication on a power-law behavior of $\psi(z)$ for both low- and high-z region is clearly observed. We assume that verification of the scaling behavior of $\psi(z)$ at even lower and higher z at high multiplicities could give new restrictions on the model parameters—the nuclear and fragmentation fractal dimensions and specific heat. A change of the parameters with the expected preservation of the slope of $\psi(z)$ at high z could be considered as a signature of a phase transition or indication of the vicinity of a critical point. Therefore quest for irregularities in the behavior of the z-scaling parameters is inspired by searching of location of a phase boundary and a critical point, which is of great interest.

Figure 13b shows the momentum fraction Ax_1 as a function of the transverse momentum of h^- hadrons produced in the most central (0–5)% Au + Au collisions for different collision energies. The momentum fractions x_1 and x_2 determine the energy of the constituent sub-process, $\sqrt{s_x}$, which underlies production of the inclusive particle with a given p_T. Using the z-presentation of the inclusive spectra of negative hadrons, we can estimate this quantity in the central Au + Au collisions at a given transverse momentum, say $p_T = 3$ GeV/c. For this purpose let us consider the collision energies $\sqrt{s_{NN}} = 7.7$, 27, and 200 GeV. As can be seen from Fig. 13b, the corresponding momentum fractions $Ax_1 (= Ax_2)$ are approximately equal to 1.11, 0.55, and 0.25. This gives the following energies $\sqrt{s_x} = 8.5$, $\sqrt{s_x} = 15$, and $\sqrt{s_x} = 50$ GeV of the underlying constituent interactions in the central Au + Au events at the considered energies, respectively. At higher energies, the medium created in the collisions of heavy nuclei becomes more hot and the energy of the underlying constituent interaction to produce a negative hadron with the given p_T increases. The increase of the energy consumption in the central collisions of heavy nuclei is a consequence of the larger energy losses in fragmentation processes and larger recoil mass in constituent sub-processes at higher $\sqrt{s_{NN}}$.

The momentum fraction y_a is a characteristic which describes energy loss in final state by production of an inclusive particle in the z-scaling scheme. The amount of energy loss and its dependence on the collision energy and transverse momentum of the produced particle has relevance to the evolution of the hadron matter created in nuclei collisions. The multiplicity dependence of the relative energy losses characterizes medium created in the collisions of nuclei, as well as fragmentation properties and structure of the probe itself. Figure 13c shows the dependence of the fraction y_a on the transverse momentum p_T for h^- hadrons produced in the most central (0–5)% Au + Au collisions for different energies. A monotonic growth of y_a with the momentum p_T is found for all energies. This means that the relative energy dissipation associated with the production of a high-p_T particle is smaller than for the inclusive processes with lower transverse momenta. At given p_T, the values of y_a decrease with the collision energy. In order to compare the energy losses in the large interval of $\sqrt{s_{NN}}$, let us consider the production of a negative hadron at $p_T = 3$ GeV/c. One can see from Fig. 13c that, at the energies $\sqrt{s_{NN}} = 7.7$, 27, and 200 GeV, the corresponding momentum fractions are $y_a = 0.82$, 0.44, and 0.13, respectively. From these values one obtains the relative energy dissipations 12, 56, and 87% when using the relation $\Delta E_q / E_q = (1 - y_a)$. The absolute energy losses, $\Delta E_q \simeq p_T(1 - y_a)/y_a$, are about $\Delta E_q = 0.7$, 3.8, and 20 GeV at the energies $\sqrt{s_{NN}} = 7.7$, 27, and 200 GeV, respectively.

As follows from the scaling behavior in the z-scaling scheme, both the relative and the absolute energy loss increases when the collision energy becomes higher. This holds also at the higher transverse momentum $p_T = 6$ GeV/c, where the relative energy dissipations amount to 45 and 83% resulting in the absolute energy loss $\Delta E_q = 4.9$ and $\Delta E_q = 29$ GeV at the energies $\sqrt{s_{NN}} = 27$ and 200 GeV, respectively. A comparison of the corresponding numbers at $p_T = 3$ and $p_T = 6$ GeV/c points to similar property as observed in the peripheral collisions. Namely, while the relative energy losses decrease with the increasing transverse momentum, the absolute energy dissipations show the opposite trend in the considered region of p_T. The ratio $\Delta E_q(p_T = 6\ \text{GeV}/c)/\Delta E_q(p_T = 3\ \text{GeV})$ of the absolute energy losses at the two considered values of transverse momentum is about 1.29 and 1.45 at the energies $\sqrt{s_{NN}} = 27$ and 200 GeV, respectively. One can see that, in the central Au + Au collisions, the increase of the absolute energy losses with p_T is considerably larger at $\sqrt{s_{NN}} = 200$ GeV than at the lower energy $\sqrt{s_{NN}} = 27$ GeV. These two numbers need to be compared with the ratios of the absolute energy losses $\Delta E_q(p_T = 6\ \text{GeV}/c)/\Delta E_q\ (p_T = 3\ \text{GeV}) = 1.2$ and 1.3, which were estimated (see Sec. 4.2.2.) for the 40–60% peripheral Au + Au collisions at $\sqrt{s_{NN}} = 27$ and 200 GeV, respectively. Based on such comparison we can make the following conclusions concerning the absolute energy dissipations: (1) The increase of the absolute energy losses with p_T is larger in the central collisions than in the peripheral ones. (2) The increase of the absolute energy losses is getting even more bigger at higher $\sqrt{s_{NN}}$ and grows significantly with the increasing centrality of the gold collisions.

The recoil mass in the underlying constituent collision, M_X, is a function of the momentum fractions x_1, x_2, y_b. The quantity is connected with the 4-momentum conservation law in the sub-process by the relation (2). The recoil mass has internal connection to the structure of the colliding objects, constituent interactions, and fragmentation processes which lead to production of the individual hadrons. The part of the recoil mass proportional to m_b is dominant for small values of y_b. Its p_T-dependence is governed by values of the fragmentation dimension ϵ_{AA}. Figure 13d shows the dependence of M_X on the transverse momentum p_T for h^- hadrons produced in the most central (0–5)% Au + Au collisions for different energies. As seen from the figure, the recoil mass increases with p_T for all collision energies and all centralities. At $p_T = 3$ GeV/c, the value of M_X is about 3.1, 4.2, and 13 GeV, at the energy $\sqrt{s_{NN}} = 7.7$, 27, and 200 GeV, respectively.

4.2.4. Cumulative region. The high density nuclear matter can be produced in cumulative processes. Production of any inclusive particle with a momentum far beyond the nucleon-nucleon kinematic region can be accompanied by cumulation of a nucleus. It is assumed that transition of the nuclear matter from the hadron to quark and gluon degrees of freedom near the critical point should reveal large fluctuations, correlations and discontinuity of some experimental quantities characterizing the system. Therefore particle production in the cumulative regions is of special interest for search for signatures of phase transition and critical point. High sensitivity of elementary constituent interactions to properties of the compressed nuclear matter is expected to be in this region [31, 32].

The cumulative processes have been extensively studied mainly in JINR (Dubna), ITEP (Moscow), IHEP (Protvino) (see [11–14, 114–116] and references therein). The results of the experiment performed in Dubna [117] on knock out deuterons from nuclei by protons were considered as an important argument in favour of the nuclear model proposed by Brueckner and his colleagues [118–120]. This model is based on the assumption that in nuclear matter strong short-range interactions exist between pairs of nucleons, in consequence of which the wave function of the ground state of the nucleus contains an appreciable admixture components corresponding to large momenta of individual nucleons. It was assumed the existence of an appreciable correlation in the locations of the nucleons inside the nuclei or short-lived formations of two or more strongly-interacting nucleons. Within the framework of the high-momentum model of the nucleus, the ejection of deuterons from nuclei by high-energy protons was considered either as the result of transfer of high momentum to the tight two-nucleon groups as a whole, or as the capture of a neutron from such a group with the formation of a deuteron emitted forward. In [121] the result obtained in [117] was connected with the fluctuations of nuclear matter. The ideas of short-range nucleon correlations and fluctuations of nuclear matter were developed in [122–129].

The first results on cumulative hadron production in heavy-ion collisions at collider mode are the data on transverse momnetum spectra obtained by the STAR collaboration in Au + Au collisions in central rapidity range at $\sqrt{s_{NN}} = 7.7$ and 11.5 GeV at the RHIC [46]. A special interest represents the study of particle production taking into account the dependence of the momentum fraction A_1x_1 on the centrality of nuclear collisions (see Figs. 12b and 13b). The fraction A_1x_1 is named as order of cumulativity or the cumulative number. The region $A_1x_1 > 1$ and/or $A_2x_2 > 1$ corresponds to the cumulative processes, indication of which is detection of a cumulative particle. The cumulative particles are particles produced in the kinematic region forbidden for free nucleon-nucleon interactions (see [11–15] and references therein). The energy of the constituent interactions with production of a cumulative particle is larger than it can be reached in the interactions on free nucleons. The cumulative particles originate from processes characterized by the order of cumulativity larger than unity. These particles are only produced in reactions with participation of nuclei.

The cumulative effect has been traditionally studied in the fixed target mode at low transverse momentum [113–116]. The soft-cumulative region typically corresponds to particle production in the backward hemisphere in laboratory frame of reference. Other approach to the cumulative effect is the investigation of hard-cumulative processes, i.e. processes with cumulative particles at high p_T [15, 130]. Study of the cumulative effect is of great interest to search for signatures of phase transitions and a critical point in highly compressed nuclear matter. Investigation of cumulative phenomena is preferred at medium energies ($\sqrt{s_{NN}} \le 20$ GeV) and with light nuclei. Such events are rare enough and the corresponding particle yields drop more the 8–10 orders of magnitude with increasing transverse momentum. It is hardly to be expected that large order of cumulativity can be experimentally reached at high collision energy. This is seen from Fig. 10b, where, except the last point in the most central collisions, the values of Ax_1 do not reach unity over the analysed range of $dN_{\text{neg}}^{\text{AuAu}}/d\eta$ and p_T at $\sqrt{s_{NN}} = 27$ GeV. The measured region at this energy is not forbidden for particle production on free nucleons. At higher collision energies, the extracted cumulative numbers are considerably less than unity (see Fig. 11b). It is clear from Figs. 12b and 13b that the cumulative region ($Ax_1 > 1$) can be realistically attain-

able at lower energy only. The registered particles at $\sqrt{s_{NN}} = 7.7$ and 11.5 GeV with $Ax_1 > 1$ are cumulative ones. The cumulative production is seen both in the central and peripheral collisions.

Let us consider the cumulative production of a negative hadron with the transverse momentum $p_T = 3$ GeV/c at the energy $\sqrt{s_{NN}} = 7.7$ GeV. For the 40–60% peripheral Au + Au collisions, the corresponding characteristics of the underlying constituent sub-process are estimated as follows (see Fig. 12): The momentum fraction $Ax_1 = 1.07$ gives the energy of the constituent interaction $\sqrt{s_x} = 8.2$ GeV. The momentum fraction $y_a = 0.84$ results in the energy loss $\Delta E_q = 0.6$ GeV. The recoil mass in the sub-process is about $M_X = 2.9$ GeV. For the 0–5% central Au + Au collisions, these characteristics change and take approximately the following values (see Fig. 13). The estimated value of the fraction $Ax_1 = 1.11$ determines the energy $\sqrt{s_x} = 8.5$ GeV of the constituent interaction which is a little bit higher. The energy loss $\Delta E_q = 0.7$ GeV, calculated from the estimate $y_a = 0.82$, increases as well. The recoil mass in the underlying sub-process $M_X = 3.1$ GeV is also a bit higher. When going from the peripheral to central collisions, the increase in the cms energy of the sub-process is shared between the increase of the energy loss and the enlargement of the recoil mass. This change is small at the energy $\sqrt{s_{NN}} = 7.7$ GeV.

Using the self-similarity assumption for the Au + Au system, we can compare the above obtained characteristics with ones corresponding to larger order of cumulativity. In this region one can investigate the structure of fluctons [121–123] (particle-like fluctuations of the nuclear matter) and fragmentation of particles produced in their interactions. It is expected that the transfer into the deeper cumulative region with high multiplicity criteria may involve an added selection of events with denser (more compressed) nuclear matter. Location of the interaction between nuclear constituents in such region allows for a direct measurement of the mass M_X, which is essentially the mass of a cumulative recoil "jet." Note that the mass of the non-registered system at low energy rises more steeply with transverse momentum (or with the order of cumulation) when compared with its increase at higher energies (see Figs. 12d and 13d). This is a consequence of the relatively large momentum fractions $A_1x_1 = A_2x_2$ and y_b in the expression for recoil mass $M_X = x_1M_1 + x_2M_2 + m_b/y_b$ when going into the cumulative region. For cumulative production, the first terms contributing to M_X become important relative to the third one. It means that the cumulative particles with high p_T are produced on larger masses (multinucleon clusters, multi-quark systems, etc.) and their transverse momentum is compensated by a relatively compact recoil system with a larger value of M_X.

To be more specific, let us examine the cumulative production of a negative hadron with the transverse momentum $p_T = 3.6$ GeV/c at the energy $\sqrt{s_{NN}} = 7.7$ GeV. For the 40–60% peripheral Au + Au collisions, the corresponding momentum fractions $Ax_1 = 1.24$ and $y_a = 0.86$ give the energy of the constituent interaction $\sqrt{s_x} = 9.5$ GeV and the absolute energy loss $\Delta E_q = 0.6$ GeV, respectively. The estimated value of the recoil mass is about $M_X = 3.2$ GeV. For the 0–5% central Au + Au collisions, the momentum fractions $Ax_1 = 1.28$ and $y_a = 0.84$ are equivalent to the energy of the constituent sub-process $\sqrt{s_x} = 9.9$ GeV and to the absolute energy loss $\Delta E_q = 0.7$ GeV, respectively. The corresponding value of the recoil mass is approximately $M_X = 3.4$ GeV. A comparison with the cumulative production at the same energy $\sqrt{s_{NN}} = 7.7$ GeV and at the lower $p_T = 3$ GeV/c shows that the absolute value of the energy loss in fragmentation processes remains the same, whereas the recoil mass increases significantly by about 0.3 GeV. These properties are independent on the centrality of Au + Au collisions.

The largest cumulative number in the production of negative hadrons from the Au + Au system was reached in the 0–5% central collisions at the energy $\sqrt{s_{NN}} = 7.7$ GeV. Its value $Ax_1 = 1.43$ corresponds to the transverse momentum $p_T = 4.2$ GeV/c. The corresponding cumulative sub-process can be considered as a hard collision of fluctons with subsequent fragmentation of particles created in their interaction. The energy of the constituent sub-process is about $\sqrt{s_x} = 11$ GeV, which is considerably higher than the energy $\sqrt{s_{NN}} = 7.7$ GeV for free nucleon-nucleon interaction. The energy of the flucton-flucton collision is consumed partially on the energy loss by production of the inclusive negative hadron and partially on the recoil mass which transforms to particles moving in the opposite direction in the medium produced in the central collisions of the gold nuclei. The absolute energy loss $\Delta E_q = 0.7$ GeV is estimated from the momentum fraction $y_a = 0.86$, which is depicted by the last cross symbol in Fig. 13c. The recoil mass is $M_X = 3.7$ GeV.

Based on the results of our analysis of the cumulative region, we make some conclusions valid both for 40–60% peripheral and 0–5% central Au + Au collisions. We observe that the absolute energy loss does not depend (or depends weekly) on the transverse momentum p_T by production of negative hadrons in the analysed cumulative region. The cumulative production is accompanied with considerable increase of

the recoil mass M_X with p_T. This behaviour is supplied by the energy of the constituent interaction which exceeds the corresponding energy for the free nucleon-nucleon collision. The relatively large increase of the recoil mass with the transverse momentum is due to the cumulative production on larger masses (particle-like fluctuations in colliding nuclei). The nearly constant value of the absolute energy loss with p_T suggests a new characteristic pattern in the fragmentation properties of cumulative particles.

We expect that, when going to the cumulative region, the fractal dimensions δ_A, ϵ_{AA} and the "specific heat" c may be sensitive to the magnitude of the cumulation. A variation in these quantities is proposed as a signature of new effects and, in particular, of a phase transition. Determining the dependence of fractal dimensions on the process cumulativity order (A_1x_1, A_2x_2), one may examine the structure of fluctons themselves (δ_A) and the properties of fragmentation (ϵ_{AA}) of particles produced in their collisions. An account of the centrality dependence of the cumulative particles yields may enhance the sensitivity of these characteristics to the order of cumulativity. It is assumed that the relation $\delta_A = A\delta$ may be violated (for example, $\delta_A = A^d\delta$, $d > 1$) in the cumulative region. The fractal dimension is expected to grow with the cumulativity order in this region: it should be greater for fluctons (the local cumulations of the nuclear matter in the nucleus) than for the ordinary nucleons in nuclei.

5. CONCLUSIONS

A review of the z-scaling concept was given. The concept is based on the fundamental symmetry principles such as the self-similarity, locality, and fractality of hadron interactions at high energies [35, 36]. In the framework of this approach, the transverse momentum spectra of inclusive particles are described in terms of the scaling function $\psi(z)$ dependent on the self-similarity parameter z. Both are expressed via measurable quantities (particle yields, multiplicity densities, momenta and masses of the colliding and produced particles) and some model parameters which allow physical interpretation. The assumption of the self-similarity of particle production transforms to the requirement of simultaneous description of the studied data sets by a dimensionless function $\psi(z)$. This gives strong constraint on the values of the model parameters and allows to determine them. We have shown results of our analysis of experimental data on transverse momentum distributions of negative hadrons, strange K^0_S, K^-, K^{*0}, ϕ mesons and Λ, Λ^*, Σ^*, Ξ, Ω baryons, top quark, and jets produced in high energy $p + p$ interactions. The z-presentation of the negative hadron spectra from Au + Au collisions measured within the STAR BES-I program at RHIC was illustrated and discussed as well.

The presented results for $p + p$ collisions support the properties of the z-scaling found in our previous analyses of inclusive spectra of different hadrons obtained at the accelerators U70, ISR, SPS, Tevatron, and RHIC. These are the energy and flavour independence of the scaling function $\psi(z)$ and universality of its shape for production of different particles in $p + p$ collisions over a wide kinematic range. The scaling function was found to be independent of the collision energy, multiplicity density, and detection angle of the produced particle. It was established that the shape of $\psi(z)$ is independent of the flavour content of inclusive hadrons in the experimentally measured region. The universality of the scaling function means that spectra of particles with different flavour content can be described by the same function $\psi(z)$ with values of z and ψ rescaled by a factor α_F. The scale factor does nod depend on kinematic variables. The multiplicative scale transformation of z and ψ with the parameter α_F allows us to reduce the scaling function for different hadrons to a single curve corresponding to $\psi(z)$ for π mesons. The function $\psi(z)$ reveals two separated regimes—in the low-z and high-z range. A power behaviour, $\psi(z) \sim z^{-\beta}$, was established in the high-z (high-p_T) range. At low z (low-p_T), a saturation of $\psi(z)$ was found [27, 28].

The energy, angular, and multiplicity independence of the scaling function gives strong constraints on the values of the model parameters c, δ, and ϵ_F entering in the definition of the scaling variable z. The parameter c is interpreted as a "specific heat" of the produced medium in the colliding system. The state of the created medium is characterized by the multiplicity density of (charged) particles in the central interaction region. The parameter c controls the behaviour of $\psi(z)$ at low z. Its value $c = 0.25$ in proton-proton collisions was established from the multiplicity independence of the scaling function. It does not depend on energy. The structure of the colliding protons at small scales is characterized by the parameter δ interpreted as a fractal dimension. It was found that, at sufficiently high energy $\sqrt{s_{NN}} \gtrsim 19.6$ GeV, the z-scaling is consistent with $\delta = 0.5$ for all types of the analysed inclusive hadrons. The fragmentation process by production of the inclusive particles is described in terms of the fragmentation dimension ϵ_F. The parameter depends on flavour content of the inclusive hadrons.

The presented results of analysis of negative hadron spectra obtained by the STAR Collaboration in the RHIC BES-I program for Au + Au collisions in the framework of the z-scaling approach support properties of data z-presentation found in our previous analyses of inclusive spectra of different particles produced in $p + p$ collisions. The scaling behaviour of the trans-

verse momentum distributions in the z-presentation as a function of the collision energy and centrality was verified. The model parameters δ_A, ϵ_{AA} and c_{AA} were found to depend on system size (or atomic number A) for $A + A$ collisions. The parameters δ_A and ϵ_{AA} characterize the fractal structure of the colliding nuclei and fractal nature of the fragmentation processes in the final state, respectively. The third parameter, c_{AA}, is interpreted as a "specific heat" of the produced medium in the $A + A$ system. The z-scaling is consistent with $c_{\mathrm{AuAu}} = 0.11$ for the analysed spectra of negative hadrons obtained from the Au + Au collisions. The values of δ_A are found to be constant, $\delta_A = 0.5A$, at sufficiently high energy $\sqrt{s_{NN}} \gtrsim 19.6$ GeV. These values do not depend on the collision centrality. The fragmentation dimension ϵ_{AA} increases with the multiplicity density. Under these conditions, described in more detail in text, the z-presentation of the inclusive spectra of negative hadrons produced in Au + Au system is independent on energy and centrality of collisions. The scaling function $\psi(z)$ reveals two regimes of behaviour—the saturation in the low-z and a power law in the high-z range. It coincides with good accuracy with the scaling function for $p + p$ interaction.

A microscopic picture of particle production in the $p + p$ and Au + Au collisions was discussed. The scenario reflects constituent structure of hadron interaction in terms of the binary sub-processes with subsequent fragmentation as a prerequisite for a unified description of particle spectra under different kinematic and dynamic conditions. This approach to hadron interactions at the constituent level is characterized in terms of the respective momentum fractions $Ax_1(Ax_2)$ and y_a of the incoming and fragmenting objects and the recoil mass M_X in the underlying constituent collisions.

These characteristics are found from the principle of minimal resolution (or equivalently maximal entropy) used in the determination of the scaling variable z. The momentum fractions depend implicitly on the fractal dimensions δ and ϵ_F which are found from the requirement of unified description of the inclusive spectra using the principle of self-similarity. In this picture, the particle production with larger values of ϵ_F is connected with larger energy losses in the final state. This implies an increase of the recoil mass M_X and consequently, the growth of the momentum fractions Ax_1 and Ax_2 in the initial state. The later determine energy of the constituent interaction which underlies production of the inclusive particle with the transverse momentum p_T. A monotonic growth of $Ax_1(= Ax_2)$, y_a and M_X with p_T was found at different collision energies for all analysed inclusive particles. Performed analysis shows that the energy losses increase with the centrality and center-of-mass energy of $p + p$ collisions following specific dependencies on the transverse momentum p_T of the inclusive particle. For the top quark and jet production the energy losses are considered as negligible. The self-similarity of proton structure and interaction of proton constituents was verified up to 10^{-4} fm in the inclusive processes with jets.

The energy loss as a function of the cms energy and centrality of Au + Au collisions in dependence on the transverse momentum of the inclusive negative hadrons was estimated. The larger values of ϵ_{AA} in the central collisions of heavy nuclei reflect larger energy losses relatively to the peripheral ones. A monotonic growth of the momentum fractions Ax_1, y_a and the recoil mass M_X with the transverse momentum p_T was found at different collision energies and for all centralities. The microscopic scenario of hadron production developed within the z-scaling approach allows us to interpret the obtained results as a formation of self-similar fractal-like objects in the dense medium created in the collisions of heavy nuclei.

The performed analysis extends applicability of the self-similarity principle to the description of hadron production in nucleus-nucleus collisions. The presented results indicate on self-similarity of fractal structure of the colliding nuclei and support the hypothesis of fractality in fragmentation processes with production of inclusive particles in the Au + Au system. A violation of such symmetry could be an indication on a change of fractal structure of hadron constituents and their interactions due to unusual properties of the nuclear medium created in $A + A$ collisions at high transverse momentum and large multiplicity density. A discontinuity of the model parameters – the structural and fragmentation fractal dimensions and "specific heat" is considered from the point of view of searching for signatures of a phase transition and a critical point in nuclear matter. Based on the obtained results we conclude that new confirmation of the scaling properties of hadron production in heavy ion collisions was found.

In summary, we conclude that the z-scaling approach can be exploited as a tool to search for and study of new physics phenomena in production of particles with different flavour content in high energy proton-proton and nucleus-nucleus collisions at the U70 (IHEP), SPS (CERN), RHIC (BNL) and LHC (CERN), and also on the future accelerators NICA (JINR) and FAIR (GSI). It can serve as a benchmark for more complex analysis of self-similar features and fractal character of hadron constituents and their interactions.

FUNDING

This work was partially supported by Project funded by the MEYS of the Czech Republic under the contract LTT18021.

REFERENCES

1. L. M. Lederman and C. T. Hill, *Symmetry and the Beautiful Universe* (Prometheus Books, New York, 2004).
2. H. E. Stanley, *Introduction to Phase Transitions and Critical Phenomena* (Oxford Univ. Press, Oxford, 1971).
3. H. E. Stanley, "Scaling, universality, and renormalization: Three pillars of modern critical phenomena," Rev. Mod. Phys. **71**, S358–S366 (1999).
4. A. Hankey and H. E. Stanley, "Systematic application of generalized homogeneous functions to static scaling, dynamic scaling, and universality," Phys. Rev. B **6**, 3515–3542 (1972).
5. S. Lübeck, "Universal scaling behavior of non-equilibrium phase transitions," Int. J. Mod. Phys. B **18**, 3977–4118 (2004).
6. R. P. Feynman, "Very high-energy collisions of hadrons," Phys. Rev. Lett. **23**, 1415–1417 (1969).
7. J. D. Bjorken, "Asymptotic sum rules at infinite momentum," Phys. Rev. **179**, 1547–1553 (1969).
8. J. D. Bjorken and E. A. Paschos, "Inelastic electron-proton and γ-proton scattering and the structure of the nucleon," Phys. Rev. **185**, 1975–1982 (1969).
9. P. Bosted, R. G. Arnold, S. Rock, and Z. Szalata, "Nuclear scaling in inelastic electron scattering from d, ^{3}He, and ^{4}He," Phys. Rev. Lett. **49**, 1380–1383 (1982).
10. J. Benecke, T. T. Chou, C. N. Yang, and E. Yen, "Hypothesis of limiting fragmentation in high-energy collisions," Phys. Rev. **188**, 2159–2169 (1969).
11. A. M. Baldin, "The physics of relativistic nuclei," Sov. J. Part. Nucl. **8**, 175–195 (1977).
12. V. S. Stavinsky, "Limiting fragmentation of nuclei-cumulative effect," Sov. J. Part. Nucl. **10**, 949–995 (1979).
13. G. A. Leksin, "Nuclear scaling. Elementary particles," in *Proc. 33rd Physics School ITEF* (Moscow, 1975), No. 2, p. 5; G. A. Leksin, "Nuclear scaling," Report No. ITEF-147 (Moscow, 1975), p. 90.
14. G. A. Leksin, in *Proceedings of the 18th International Conf. on High Energy Physics, Tbilisi, USSR, 1976,* Ed. by N. N. Bogolubov et al. (JINR, D1, 2-10400, Tbilisi, 1977), p. A6-3.
15. G. A. Leksin, "Methods for investigating nuclear matter under the conditions characteristic of its transition to quark-gluon plasma," Phys. At. Nucl. **65**, 1985–1994 (2002).
16. Z. Koba, H. B. Nielsen, and P. Olesen, "Scaling of multiplicity distributions in high-energy hadron collisions," Nucl. Phys. B **40**, 317–334 (1972).
17. A. M. Polyakov, "A similarity hypothesis in the strong interactions. I. Multiple hadron production in e^+e^--annihilation," Sov. Phys **32**, 296–301 (1971).
18. A. M. Polyakov, "A similarity hypothesis in the strong interactions. II. Cascade production of hadrons and their energy distribution associated with e^+e^--annihilation," Sov. Phys. JETP **33**, 850–855 (1971).
19. V. A. Matveev, R. M. Muradyan, and A. N. Tavkhelidze, "Automodelity, current algebra and vector dominance in deep inelastic lepton-hadron interactions," Part. Nucl. **2**, 5–32 (1971).
20. V. A. Matveev, R. M. Muradyan, and A. N. Tavkhelidze, "Automodelity in strong interactions," Lett. Nuovo Cim. **5**, 907–912 (1972).
21. V. A. Matveev, R. M. Muradyan, and A. N. Tavkhelidze, "Automodellism in the large-angle elastic scattering and structure of hadrons," Lett. Nuovo Cim. **7**, 719–723 (1973).
22. S. J. Brodsky and G. R. Farrar, "Scaling laws at large transverse momentum," Phys. Rev. Lett. **31**, 1153–1156 (1973).
23. S. J. Brodsky and G. R. Farrar, "Scaling laws for large-momentum-transfer processes," Phys. Rev. D: Part. Fields **11**, 1309–1330 (1975).
24. L. Nottale, *Fractal Space-Time and Microphysics: Towards a Theory of Scale Relativity* (World Sci., 1993).
25. L. Nottale, "Scale relativity and fractal space-time: Theory and applications," Found. Sci. **15**, 101–152 (2010).
26. L. Nottale, *Scale Relativity and Fractal Space-Time: a New Approach to Unifying Relativity and Quantum Mechanics* (World Sci., 2011).
27. I. Zborovský and M. V. Tokarev, "Generalized z-scaling in proton-proton collisions at high energies," Phys. Rev. D: Part. Fields **75**, 094008 (2007).
28. I. Zborovský and M. V. Tokarev, "New properties of z-scaling: Flavor independence and saturation at low z," Int. J. Mod. Phys. A **24**, 1417–1442 (2009).
29. M. V. Tokarev and T. G. Dedovich, "z-Scaling and jet production in hadron-hadron collisions at high energies," Int. J. Mod. Phys. A **15**, 3495–3519 (2000).
30. M. V. Tokarev, I. Zborovský, and T. G. Dedovich, "Self-similarity of jet production in $p + p$ and $p + \bar{p}$ collisions at RHIC, tevatron and LHC," Int. J. Mod. Phys. A **27**, 1250115 (2012).
31. M. V. Tokarev and I. Zborovský, "Self-similarity of high-p_T hadron production in pp and $p\bar{p}$ cumulative processes and violation of discrete symmetries at small scales (suggestion for experiment)," Phys Part. Nucl. Lett. **7**, 160–170 (2010).
32. M. V. Tokarev, I. Zborovský, A. O. Kechechyan, and A. Alakhverdyants, "Search for signatures of phase transition and critical point in heavy-ion collisions," Phys Part. Nucl. Lett. **8**, 533–541 (2011).
33. M. V. Tokarev and I. Zborovský, "Energy scan in heavy-ion collisions and search for a critical point," Phys. At. Nucl. **75**, 700–706 (2012).
34. M. V. Tokarev and I. Zborovský, "On self-similarity of top production at tevatron," Int. J. Mod. Phys. A **3**, 815–820 (2012).
35. M. V. Tokarev and I. Zborovský, "z-Scaling as manifestation of symmetry in Nature," in *Selected Papers of the Seminar (2002–2005), "Symmetries and Integrable*

Systems", Ed. by A. N. Sysakian (JINR, Dubna, 2006), Vol. 2, p. 154.

36. M. V. Tokarev and I. Zborovský, "Self-similarity of hadron production: z-scaling," Theor. Math. Phys. **184**, 530–543 (2015).
37. M. V. Tokarev, "z-Scaling at RHIC," Phys. Part. Nucl. Lett. **3**, 7–17 (2006).
38. M. V. Tokarev, "Scaling in heavy ion collisions at the RHIC," Phys. Part. Nucl. Lett. **4**, 403–414 (2007).
39. M. V. Tokarev and I. Zborovský, "Self-similarity of pion production in AA collisions at RHIC," Phys. Part. Nucl. Lett. **7**, 171–184 (2010).
40. M. V. Tokarev (for the STAR Collab.), "High-p_T spectra of charged hadrons in Au+Au collisions at $\sqrt{s_{NN}}$ = 9.2 GeV in STAR," Phys. At. Nucl. **74**, 799–804 (2011).
41. M. V. Tokarev and I. Zborovský, "Beam energy scan at RHIC and z-scaling," Nucl. Phys. B Proc. Suppl. **245**, 231–238 (2013).
42. M. V. Tokarev and I. Zborovský, "Energy loss in heavy ion collisions," in *Proc. 40th Int. Symp. on Multiparticle Dynamics (ISMD 2010)* (Antwerp, Sept. 21–25, 2010), p. 301.
43. I. Zborovský, Yu. A. Panebratsev, M. Tokarev, and G. Škoro, "Z scaling in hadron-hadron collisions at high energies," Phys. Rev. D: Part. Fields **54**, 5548–5557 (1996).
44. M. V. Tokarev, I. Zborovský, Yu. Panebratsev, and G. Škoro, "A-dependence of z-scaling," Int. J. Mod. Phys. A **16**, 1281–1302 (2001).
45. M. V. Tokarev and I. Zborovský, "Multiplicity dependence of z scaling for identified hadrons," Phys. Atom. Nucl. **70**, 1294–1304 (2007).
46. M. V. Tokarev (for the STAR Collab.), "Self-similarity of negative particle production from the beam energy scan program at STAR," Int. J. Mod. Phys. Conf. Ser. **39**, 1560103 (2015).
47. M. V. Tokarev and I. Zborovský, "New indication on scaling properties of strangeness production in $p + p$ collisions at RHIC," Int. J. Mod. Phys. A **32**, 1750029 (2017).
48. B. I. Abelev et al. (STAR Collab.), Experimental study of the QCD phase diagram & search for the critical point: Selected arguments for the Run-10 beam energy scan (June 4, 2009). http://drupal.star.bnl.gov/STAR/starnotes/public/sn0493.
49. B. I. Abelev et al. (STAR Collab.), "Identified particle production, azimuthal anisotropy, and interferometry measurements in Au + Au collisions at $\sqrt{s_{NN}}$ = 9.2 GeV," Phys. Rev. C **81**, 024911 (2010).
50. STAR Collab., "Studying the phase diagram of QCD matter at RHIC," STAR Note SN0598 (June 1, 2014).
51. V. V. Abramov et al., "Hadron production at transverse momenta from 0.5 GeV/c up to 2.2 GeV/c in proton proton collisions at 70 GeV," Nucl. Phys. B **173**, 348–364 (1980).
52. V. V. Abramov et al., "Production of charged hadrons with large transverse momenta in pp collisions at 70 GeV," JETP Lett. **33**, 289–293 (1981).
53. D. Antreasyan et al., "Production of hadrons at large transverse momentum in 200-, 300-, and 400-GeV p–p and p–nucleus collisions," Phys. Rev. D: Part. Fields **19**, 764–778 (1979).
54. D. E. Jaffe et al., "High-transverse-momentum single-hadron production in pp and pd collisions at $\sqrt{s_{NN}}$ = 27.4 and 38.8 GeV," Phys. Rev. D: Part. Fields **40**, 2777–2795 (1989).
55. A. Breakstone et al. (ABCDHW Collab.), "Inclusive charged particle cross-sections in full phase space from proton–proton interactions at ISR energies," Z. Phys. C **69**, 55–66 (1995).
56. D. Drijard et al. (CDHW Collab.), "A measurement of the inclusive cross-section of charged pions at very high transverse momenta," Nucl. Phys. B **208**, 1–11 (1982).
57. G. Agakishiev et al. (STAR Collab.), "Identified hadron compositions in $p + p$ and Au + Au collisions at high transverse momenta at $\sqrt{s_{NN}}$ = 200 GeV," Phys. Rev. Lett. **108**, 072302 (2012).
58. B. I. Abelev et al. (STAR Collab.), "Strange particle production in $p + p$ collisions at $\sqrt{s_{NN}}$ = 200 GeV," Phys. Rev. C **75**, 064901 (2007).
59. J. Adams et al. (STAR Collab.), "K(892)* resonance production in Au + Au and $p + p$ collisions at $\sqrt{s_{NN}}$ = 200 GeV at STAR," Phys. Rev. C **71**, 064902 (2005).
60. A. Adare et al. (PHENIX Collab.), "Measurement of K_s^0 and K^{*0} in $p + p$, d + Au, and Cu + Cu collisions at $\sqrt{s_{NN}}$ = 200 GeV," Phys. Rev. C **90**, 054905 (2014).
61. A. Adare et al. (PHENIX Collab.), "Measurement of neutral mesons in $p + p$ collisions at $\sqrt{s_{NN}}$ = 200 GeV and scaling properties of hadron production," Phys. Rev. D: Part. Fields **83**, 052004 (2011).
62. B. I. Abelev et al. (STAR Collab.), "Strange baryon resonance production in $\sqrt{s_{NN}}$ = 200 GeV p+p and Au + Au collisions," Phys. Rev. Lett. **97**, 132301 (2006).
63. J. Adams et al. (STAR Collab.), "Identified hadron spectra at large transverse momentum in $p + p$ and d + Au collisions at $\sqrt{s_{NN}}$ = 200 GeV," Phys. Lett. B **637**, 161–169 (2006).
64. B. Alper et al. (BS Collab.), "Production spectra of $\pi^{\pm}$, $K^{\pm}$, $p^{\pm}$ at large angles in proton-proton collisions in the CERN Intersecting Storage Rings," Nucl.Phys. B **100**, 237–290 (1975).
65. F. W. Busser et al., "K^0 and Λ production at the CERN ISR," Phys. Lett. B **61**, 309–312 (1976).
66. H. Kichimi et al., "Inclusive study of strange particle production in p–p interactions at 405 GeV/c," Phys. Rev. D **20**, 37–52 (1979).
67. D. Drijard et al., "Neutral strange particle production in proton-proton collisions at $\sqrt{s_{NN}}$ = 63 GeV," Z. Phys. C **12**, 217–224 (1982).
68. T. Akesson et al. (AFS Collab.), "Inclusive vector-meson production in the central region of $p + p$ collisions at $\sqrt{s_{NN}}$ = 63 GeV," Nucl. Phys. B **203**, 27–39 (1982); Nucl. Phys. B **229**, 541(E) (1983).

69. A. Aduszkiewicz et al. (NA61/SHINE Collab.), "Production of Λ-hyperons in inelastic $p + p$ interactions at 158 GeV/c," Eur. Phys. J. C **76**, 198 (2016).

70. S. V. Afanasiev et al. (NA49 Collab.), "Production of φ mesons in $p + p$, $p +$ Pb and central Pb +Pb collisions at $E_{\text{beam}} = 158\,A$ GeV," Phys. Lett. B **491**, 59–66 (2000).

71. T. Anticic et al. (NA49 Collab.), "$K^*(892)^0$ and $\bar{K}^*(892)^0$ production in central Pb + Pb, Si + Si, C + C, and inelastic $p + p$ collisions at 158 A GeV," Phys. Rev. C **84**, 064909 (2011).

72. J. Adams et al. (STAR Collab.), "ϕ meson production in Au + Au and $p + p$ collisions at $\sqrt{s_{NN}} = 200$ GeV," Phys. Lett. B **612**, 181–189 (2005).

73. F. Abe et al. (CDF Collab.), "Observation of top quark production in $p\bar{p}$ collisions with the Collider Detector at Fermilab," Phys. Rev. Lett. **74**, 2626–2631 (1995).

74. S. Abachi et al. (DØ Collab.), "Observation of the top quark," Phys. Rev. Lett. **74**, 2632–2637 (1995).

75. V. M. Abazov et al. (DØ Collab.), "Dependence of the $t\bar{t}$ production cross section on the transverse momentum of the top quark," Phys. Lett. B **693**, 515–521 (2010).

76. S. Chatrchyan et al. (CMS Collab.), "Measurement of differential top-quark pair production cross sections in pp colisions at $\sqrt{s} = 7$ TeV," Eur. Phys. J. C **73**, 2339 (2013).

77. V. Khachatryan et al. (CMS Collab.), "Measurement of the differential cross section for top quark pair production in pp collisions at $\sqrt{s} = 8$ TeV," Eur. Phys. J. C **75**, 542 (2015).

78. V. Khachatryan et al. (CMS Collab.), "Measurement of the integrated and differential $t\bar{t}$ production cross sections for high-pt top quarks in pp collisions at $\sqrt{s} =$ 8 TeV," Phys. Rev. D: Part. Fields **94**, 072002 (2016).

79. CMS Collab., "Measurement of the differential cross section for $t\bar{t}$ production in the dilepton final state at $\sqrt{s} = 13$ TeV," CMS PAS TOP-16-011.

80. G. Aad et al. (ATLAS Collab.), "Measurements of normalized differential cross sections for $t\bar{t}$ production in pp collisions at $\sqrt{s} = 7$ TeV using the ATLAS detector," Phys. Rev. D: Part. Fields **90**, 072004 (2014).

81. G. Aad et al. (ATLAS Collab.), "Differential top-antitop cross-section measurements as a function of observables constructed from final-state particles using pp collisions at $\sqrt{s} = 7$ TeV in the ATLAS detector," J. High Energy Phys. **06**, 100 (2015).

82. G. Aad et al. (ATLAS Collab.), "Measurement of the differential cross-section of highly boosted top quarks as a function of their transverse momentum in $\sqrt{s} =$ 8 TeV proton-proton collisions using the ATLAS detector," Phys. Rev. D: Part. Fields **93**, 032009 (2016).

83. G. Aad et al. (ATLAS Collab.), "Measurements of top-quark pair differential cross-sections in the lepton + jets channel in pp collisions at $\sqrt{s} = 8$ TeV using the ATLAS detector," Eur. Phys. J. C **76**, 538 (2016).

84. V. M. Abazov et al. (DØ Collab.), "Measurement of differential production cross sections in $p\bar{p}$ collisions," Phys. Rev. D: Part. Fields **90**, 092006 (2014).

85. G. Aad et al. (ATLAS Collab.), "Measurement of the inclusive jet cross-section in pp collisions at $\sqrt{s} =$ 2.76 TeV and comparison to the inclusive jet cross-section at $\sqrt{s} = 7$ TeV using the ATLAS detector," Eur. Phys. J. C **73**, 2509 (2013).

86. B. Abelev et al. (ALICE Collab.), "Measurement of the inclusive differential jet cross section in pp collisions at $\sqrt{s} = 2.76$ TeV," Phys. Lett. B **722**, 262–272 (2013).

87. CMS Collab., "Measurement of the double-differential inclusive jet cross section at $\sqrt{s} = 8$ TeV with the CMS detector," PAS-SMP-12-012.

88. M. Aaboud et al. (ATLAS Collab.), "Measurement of the inclusive jet cross-sections in proton-proton collisions at $\sqrt{s} = 8$ TeV with the ATLAS detector," J. High Energy Phys. **09**, 020 (2017).

89. V. M. Abazov et al. (DØ Collab.), "Measurement of the inclusive jet cross section in $p\bar{p}$ collisions at $\sqrt{s} =$ 1.96 TeV," Phys. Rev. D: Part. Fields **85**, 052006 (2012).

90. A. Abulencia et al. (CDF Collab.), "Measurement of the inclusive jet cross section using the k_T algorithm in $p\bar{p}$ collisions at $\sqrt{s} = 1.96$ TeV," Phys. Rev. Lett. **96**, 122001 (2006).

91. A. Abulencia et al. (CDF Collab.), "Measurement of the inclusive jet cross section in $p\bar{p}$ interactions at $\sqrt{s} = 1.96$ TeV using a cone-based jet algorithm," Phys. Rev. D: Part. Fields **74**, 071103(R) (2006).

92. A. Abulencia et al. (CDF Collab.), "Measurement of the inclusive jet cross section using the k_T algorithm in $p\bar{p}$ collisions at $\sqrt{s} = 1.96$ TeV with the CDF II detector," Phys. Rev. D: Part. Fields **75**, 092006 (2007).

93. T. Aaltonen et al. (CDF Collab.), "Measurement of the inclusive jet cross section at the Fermilab Tevatron $p\bar{p}$ collider using a cone-based jet algorithm," Phys. Rev. D: Part. Fields **78**, 052006 (2008); Phys. Rev. D **79**, 119902(E) (2009).

94. S. Chatrchyan et al. (CMS Collab.), "Measurements of differential jet cross sections in proton-proton collisions at $\sqrt{s} = 7$ TeV with the CMS detector," Phys. Rev. D: Part. Fields **87**, 112002 (2013).

95. G. Aad et al. (ATLAS Collab.), "Measurement of inclusive jet and dijet production in pp collisions at $\sqrt{s} =$ 7 TeV using the ATLAS detector," Phys. Rev. D: Part. Fields **86**, 014022 (2012).

96. B. Abbott et al. (DØ Collab.), "High-p_T jets in $p\bar{p}$ collisions at $\sqrt{s} = 630$ GeV and 1800 GeV," Phys. Rev. D: Part. Fields **64**, 032003 (2001).

97. V. D. Elvira, "Measurement of the inclusive jet cross sections at $\sqrt{s} = 1.8$ TeV with the DØ detector," Ph.D Thesis (Universodad de Buenos Aires, 1995).

98. V. M. Abazov et al. (DØ Collab.), "The inclusive jet cross section in $p\bar{p}$ collisions at $\sqrt{s} = 1.8$ TeV using the $k_\perp$ algorithm," Phys. Lett. B **525**, 211–218 (2002).
99. V. M. Abazov et al. (DØ Collab.), "Measurement of the inclusive jet cross section in $p\bar{p}$ collisions at $\sqrt{s} =$ 1.96 TeV," Phys. Rev. Lett. **101**, 062001 (2008).
100. M. Begel (for the DØ Collab.), Jet mmeasurements at $\sqrt{s} = 1.96$ TeV; arXiv:hep-ex/0305072.
101. F. Abe et al. (CDF Collab.), "Inclusive jet cross section in $p\bar{p}$ collisions at $\sqrt{s} = 1.8$ TeV," Phys. Rev. Lett. **77**, 438–443 (1996).
102. T. Affolder et al. (CDF Collab.), "Measurement of the inclusive jet cross section in $p\bar{p}$ collisions at $\sqrt{s} =$ 1.8 TeV," Phys. Rev. D: Part. Fields **64**, 032001 (2001).
103. J. Cleymans, H. Oeschler, K. Redlich, and S. Wheaton, "Comparison of chemical freeze-out criteria in heavy-ion collisions," Phys. Rev. C **73**, 034905 (2006).
104. S. Wheaton, J. Cleymans, and M. Hauer, "THERMUS: A thermal model package for ROOT," Comput. Phys. Commun. **180**, 84–106 (2009).
105. A. Andronic, P. Braun-Munzinger, and J. Stachel, "Hadron production in central nucleus-nucleus collisions at chemical freeze-out," Nucl. Phys. A **772**, 167–199 (2006).
106. A. Andronic, P. Braun-Munzinger, and J. Stachel, "The horn, the hadron mass spectrum and the QCD phase diagram: The statistical model of hadron production in central nucleus-nucleus collisions," Nucl. Phys. A **834**, 237C (2010).
107. F. Becattini, J. Manninen, and M. Gazdzicki, "Energy and system size dependence of chemical freeze-out in relativistic nuclear collisions," Phys. Rev. C **73**, 044905 (2006).
108. M. M. Aggarwal et al. (STAR Collab.), An experimental exploration of the QCD phase diagram: The search for the critical point and the onset of deconfinement. arXiv:1007.2613.
109. L. Kumar (for the STAR Collab.), "Bulk properties in Au + Au collisions at $\sqrt{s_{NN}} = 9.2$ GeV in STAR experiment at RHIC," Nucl. Phys. A **830**, 275C–278C (2009).
110. B. Mohanty (for the STAR Collab.), "QCD phase diagram: Phase transition, critical point and fluctuations," Nucl. Phys. A **830**, 899C–907C (2009).
111. L. Kumar (for the STAR Collab.), "Results from the STAR beam energy scan program," Nucl. Phys. A **862–863**, 123–131 (2011).
112. L. Adamczyk et al. (STAR Collab.), "Bulk properties of the medium produced in relativistic heavy-ion collisions from the beam energy scan program," Phys. Rev. C **96**, 044904 (2017).
113. N. A. Nikiforov et al., "Backward production of pions and kaons in the interaction of 400 GeV protons with nuclei," Phys. Rev. C **C22**, 700–710 (1980).
114. O. P. Gavrishchuk et al., "Charged pion backward production in 15–65 GeV proton–nucleus collisions," Nucl. Phys. A **523**, 589–596 (1991).
115. I. M. Belyaev et al., "Production of cumulative pions and kaons in proton-nucleus interactions at energies from 15 to 65 GeV," Yad. Fiz. **56**, 135–152 (1993).
116. V. K. Bondarev, "Cumulative production of particles on proton and nucleus beams," Phys. Part. Nucl. **28**, 5–36 (1997).
117. L. S. Azhgirei et al., "Knock out deutrons from Li, Be, C and O nuclei by protons of energy 675 MeV," Zh. Eksp. Teor. Fiz. **33**, 1185–1195 (1957).
118. K. Brueckner and C. Levinson, "Approximate reduction of the many-body problem for strongly interacting particles," Phys. Rev. **97**, 1344–1352 (1955).
119. K. Brueckner, "Two-body forces and nuclear saturation. III. Details of the structure of the nucleus," Phys. Rev. **97**, 1353–1366 (1955).
120. K. Brueckner, "Many-body problem for strongly interacting particles. II. Linked cluster expansion," Phys. Rev. **100**, 36–45 (1955).
121. D. I. Blokhintsev, "On the fluctuations of nuclear matter," Sov. Phys. JETP **6**, 995–999 (1958).
122. V. V. Burov, V. K. Lukyanov, and A. I. Titov, "Large momentum pion production in proton nucleus collisions and the idea of "fluctuons" in nuclei," Phys. Lett. B **67**, 46–48 (1977).
123. V. K. Lukyanov and A. I. Titov, "Nuclear reactions with large momentum transfer and hypothesis of "fluctons" in nuclei," Fiz. Elem. Chast. Atom. Yadra **10**, 815–849 (1979).
124. L. L. Frankfurt and M. I. Strikman, "High-energy phenomena, short-range nuclear structure and QCD," Phys. Rep. **76**, 215–347 (1981).
125. L. L. Frankfurt and M. I. Strikman, "Hard nuclear processes and microscopic nuclear structure," Phys. Rep. **160**, 235–427 (1988).
126. A. V. Efremov, "Quark-parton picture of cumulative production," Sov. J. Part. Nucl. **13**, 254–263 (1982).
127. A. V. Efremov, A. B. Kaidalov, V. T. Kim, et al., "Cumulative hadron production in quark models of fluctuon fragmentation," Sov. J. Nucl. Phys. **47**, 1364–1374 (1988).
128. M. A. Braun and V. V. Vechernin, "Cumulative phenomena in the QCD approach," Nucl. Phys. B. Proc. Suppl. **92**, 156–161 (2001).
129. A. A. Baldin and A. M. Baldin, "Relativistic nuclear physics: Relative 4-velocity space, symmetries of solutions, correlation depletion principle, similar attitude, intermediate asymptotics," Phys. Part. Nucl. **29**, 232–253 (1998).
130. V. V. Ammosov et al., "Measurement of the yields of positively charged particles at an angle of 35° in proton interactions with nuclear targets at an energy of 50 GeV," Phys. At. Nucl. **76**, 1213–1218 (2013).